Silver 4,4′-vinylenedipyridine coordination polymers: linker effects on formation thermodynamics and anion exchange

Jeremy L. Barnett, John S. Wenger, Addis Getahun, Timothy C. Johnstone and Scott R. J. Oliver*

Department of Chemistry and Biochemistry, University of California, Santa Cruz, CA, 95064, USA

*Email: soliver@ucsc.edu

Abstract:
Four new and one previously reported silver 4,4′-vinylenedipyridine (Vpe) coordination polymers were tested as anion exchange materials to assess their potential for pollutant sequestration and compared to analogous silver 4,4′-bipyridine (bipy) coordination polymers. The materials were synthesized using nitrate, tetrafluoroborate, perchlorate, perrhenate or chromate as the anion to produce cationic coordination polymers with solubilities ranging from 0.0137(7) to 0.21(5) mM. These values are much lower than silver bipy coordination polymers [0.045(3) to 5.5(5) mM] and agree with thermochemical calculations. $[Ag(Vpe)^+][BF_4^-]$, $[Ag_2(Vpe)_{2.5}^{2+}][CrO_4^{2-}]\cdot 5H_2O$ and $[Ag(Vpe)^+][ReO_4^-]\cdot 2H_2O$ structures are reported. Perrhenate and chromate ions in an equimolar solution were fully adsorbed by $[Ag(Vpe)^+][NO_3^-]\cdot 3H_2O$ [620(2) and 137.1(6) mg/g, respectively] as well as by $[Ag(Vpe)^+][BF_4^-]$ [661.8(3) and 190(3) mg/g, respectively] *via* anion exchange. DFT calculations show torsional energetics play a significant role in the formation thermodynamics by reducing the energy cost by as much as 4.8 kJ/mol when bipy is replaced with Vpe in silver-based coordination polymers. The results obtained with the flat Vpe ligand highlight the potential role for coordination polymers in practical anion exchange.

Keywords: anion exchange, cationic coordination polymer, aqueous formation energy, torsion, dihedral, ligand stacking

Introduction:

Anion exchange materials are used to remove toxic pollutants such as perchlorate (ClO_4^-),[1–8] chromate (CrO_4^{2-}),[9,10] dichromate ($Cr_2O_7^{2-}$),[9] arsenate (AsO_4^{3-}), perrhenate (ReO_4^-)[11–15] and radioactive pertechnetate (TcO_4^-)[11,14,16–18] from water. Commercial polymer resins currently used for ion exchange are challenged by lack of economical regenerability and in some cases reduced specificity due to competitive binding by prominent anions present in natural water including Cl^-, SO_4^{2-}, Br^-, F^-, HCO_3^- amongst others.[19–21] Metal-organic coordination polymers (CPs) offer a possible solution with high exchange selectivity and regenerative abilities.[1–3,10–12,22–41] Their uptake capacity and sorption kinetics are competitive with commercial ion exchange resins and comparable materials.[1,3,26,42] Fully inorganic alternatives such as layered

double hydroxides (LDHs) have their practical use but suffer from selectivity and lower adsorption capacities.[1] CPs have features of both fully inorganic and fully organic anion exchangers, allowing for high modularity.

CPs have a cationic metal node bound to a polydentate ligand forming 1D, 2D or 3D structures.[43] Depending on the charge of the ligand and the oxidation state of the metal, neutral, cationic or anionic frameworks can be formed. Neutral frameworks are often formed with carboxylate functional groups whereas cationic CPs are typically formed using neutral nitrogen heterocycles. The nitrogen heterocycles form dative bonds between the metal node and the nitrogen lone pair. Interstitial anions function as charge-balancing, space-filling and structure-directing agents. Silver(I) cations with the linear bidentate ligands form 1D CPs due to the silver d^{10} closed subshell and empty s-orbital, preferring a linear coordination geometry.[44] 2D and 3D silver CPs of similar composition have been reported with multi-bridging ligands.[45,46] 1D CPs formed by silver cations with linear μ-2 bridging ligands exhibit efficient anion exchange through crystal-to-crystal transformations.[3,23,26,47] CPs with other metals such as zinc or cadmium, or those with silver in a non-linear geometry, also display ion exchange through crystal-to-crystal transformations.[33,37,41,48]

Previous work on anion exchanging 1D silver bipy coordination polymers showed high anion selectivity, fast kinetics and high adsorption capacity for perchlorate, outperforming LDHs and cationic resins with 353.97, 47.51 and 103.88 mg ClO_4^- per gram of material, respectively.[1,26] LDHs have been reported to uptake ClO_4^- as high as 99.85 mg/g.[49,50] LDHs anion exchange capacities for ReO_4^- are 93 mg/g[51] and 127.7[52] mg/g and can range from 17.0 to 726 mg/g[53–55] for Cr(IV) oxyanions including CrO_4^{2-}, depending on the conditions and LDH used. Schröder *et al.*[56] showed an interdependence between the metal [Zn(II), Ag(I), Hg(II) or Cd(II)], ligand [4,4;-bipyridine, pyrazine, 3, 4′-bipyridine or 9,10-bis(4-pyridyl)anthracene] and anion (NO_3^-, $CF_3SO_3^-$, CH_3COO^-, Cl^-, BF_4^- or ClO_4^-), which altered the solubility, structure morphology and anion exchange preference. A review by Adarsh *et al.*[57] illustrated the crystal geometry and morphology directing function of the CP ligand though pyridyl modification. Citrak *et al.*[26] showed the correlation between the solubility product constant (K_{sp}) and the hierarchy of the anion exchange order for silver bipy CPs, suggesting a thermodynamic dependency. One drawback of using silver bipy CPs is the relatively high solubility of the exchange product, represented by a relatively low magnitude Gibbs free energy of formation (ΔG_f) from solution. Increasing the magnitude (more negative) of ΔG_f of the anion exchange product will result in an increase in anion sequestration stability, lower residual anion concentration and increased product yields. Such improved thermodynamic stability will also assist in outcompeting common anions such as halides, which form silver halides with comparable ΔG_f. Understanding the factors influencing thermodynamic properties, such as ΔG_f and the resultant equilibrium aqueous concentration, is crucial for enhancing anion uptake efficiency.

Linker substitution has been shown to influence the CP thermodynamics[56,58] and thus can alter the anion exchange properties. Bipy tends to exhibit a high dihedral angle between the two pyridine rings (up to ~ 35°) in both gas phase density functional theory (DFT) calculations and single crystal data (neat bipy and bipy hydrates).[59,60] CPs with

bipy display a reduction in the dihedral angle compared to molecular bipy. Based on this observation, we hypothesized that CP crystals thermodynamically favor a flatter ligand. Previous reports suggest that ligand rigidification and reduced dihedral angle can improve 3D metal organic framework thermodynamic stability;[61–65] however, similar investigations of the effects of ligand rigidification and dihedral angle in 1D cationic CPs for anion exchange applications is lacking. We sought to employ Vpe, a flatter and longer ligand relative to bipy, as an organic linking agent to elucidate the effect of ligand rigidity and geometry on silver coordination polymers and their solution thermodynamics, aiming to improve water purification and aqueous pollutant sequestration technologies. Our goal is to advance the understanding of chemical and thermodynamic factors governing selectivity and adsorption capacity, towards a potential rational design of effective anion removal materials.

Here, we present four new cationic CPs: silver Vpe tetrafluoroborate (SVB) $[Ag(Vpe)^+][BF_4^-]$; silver Vpe perchlorate (SVP) $[Ag(Vpe)^+][ClO_4^-]$; silver Vpe perrhenate (SVR) $[Ag(Vpe)^+][ReO_4^-]\cdot 2H_2O$; and silver Vpe chromate (SVC) $[Ag_2(Vpe)_{2.5}^{2+}][CrO_4^{2-}]\cdot 5H_2O$. The crystal structures of SVB, SVR and SVC are discussed. These four new CPs and the previously reported silver Vpe nitrate (SVN) ($[Ag(Vpe)^+][NO_3^-]\cdot 3H_2O$) were compared to existing bipy CPs, showing an increase in thermodynamic aqueous stability and thus superior anion sequestering ability.

Experimental:

Reagents: Silver acetate ($AgCH_3CO_2$, Fisher Chemical, 98%) silver nitrate ($AgNO_3$, CHEM-IMPEX, 99.96%), silver tetrafluoroborate ($AgBF_4$, Oakwood Chemical, 99%), silver perchlorate hydrate ($AgClO_4\cdot xH_2O$, Aldrich Chemistry, 99%), ammonium perrhenate (NH_4ReO_4, Thermo Scientific, 99+%), potassium chromate (K_2CrO_4, Fisher Chemical, 99.9%), 4,4′-vinylenedipyridine [Vpe, $C_{12}H_{10}N_2$, Combi-Blocks, 98%; synonyms: 1,2-di(4-pyridyl)ethylene, 1,2-bis(4-pyridyl)ethylene], 4,4′-bipyridine ($C_{10}H_8N_2$, TCI, > 98.0%) and silver oxide (Ag_2O, Thermo Scientific, 99+%). Milli-Q water (< 18.2 $M\Omega\cdot cm^{-1}$), formic acid (CH_2O_2, Thermo Scientific, 85%), ammonium hydroxide (NH_4OH, Fisher Scientific, Reagent ACS, 29.7%), sodium hydroxide (NaOH, VWR, 1.000 N) and 2-propanol (C_3H_7OH, Fisher Chemical, HPLC grade) liquid reagents were used as received. Metal salts were dehydrated under vacuum prior to use in synthesis.

Synthesis: Coordination polymers $[Ag(Vpe)^+][BF_4^-]$, SVB, which we denote as SLUG-63, for University of California, Santa Cruz, Structure No. 63 and $[Ag(Vpe)^+][ClO_4^-]$, SVP, were synthesized using 0.3 mmol of the corresponding silver salt and Vpe in a 1:1 molar ratio in 25 mL of Milli-Q water. Stirring at room temperature over 24 h produced white powders. High quality single crystal needles of SVB were synthesized using 0.3 mmol of silver tetrafluoroborate and Vpe in 25 mL of water, 5 mL of methanol, 5 mL of 2-propanol and 3 mL of ammonium hydroxide. Subsequent sonication resulted in a clear solution and that was allowed to slowly evaporate over a week. Coordination polymer

$[Ag(Vpe)^+][NO_3^-]\cdot 3H_2O$, SVN, was synthesized by the same method as SVB and SVP, with the addition 5 mL of 2-propanol and 3 mL of ammonium hydroxide to produce a white microcrystalline powder. Coordination polymers SLUG-64, $[Ag(Vpe)^+][ReO_4^-]\cdot 2H_2O$, SVR and SLUG-65, $[Ag_2(Vpe)_{2.5}^{2+}][CrO_4^{2-}]\cdot 5H_2O$, SVC, were synthesized using Vpe, anion salt (0.3 mmol) in 1:1 molar ratio in 25 mL Milli-Q water followed by the addition of excess silver diamine $[Ag(NH_3)_2^+][OH^-]$ saturated aqueous solution. SVR was placed in a refrigerator for slow evaporation which produced white needles of single crystal quality. SVC was allowed to evaporate at room temperature, producing yellow square platelets of single crystal quality. $[Ag(NH_3)_2^+][OH^-]$ solution was synthesized by dissolving silver oxide in 29.7% ammonium hydroxide. Resultant powders of the CPs were vacuum filtered and rinsed with Milli-Q water. Single crystal quality products were not filtered and instead stored in their mother liquor.

Solubility: The CP was rinsed by adding ~ 15 mL of Milli-Q water followed by manual shaking, vortexing, 5 min of sonication and finally centrifugation. The supernatant was decanted, and the process was repeated two more times. The final pellet was vacuum filtered. 15 mg of the rinsed CP was added to 15 mL of Milli-Q water in a screw capped tube and manually shaken. The solution was allowed to sit for a minimum of 7 d in the dark, shaking once per day to reach solubility equilibrium. 0.5 mL aliquots were removed and filtered using a 0.45 μm syringe filter. Silver ion concentration in the filtrate was determined using a Thermo Scientific iCAP 7400 inductively coupled plasma optical emission spectrometer (ICP-OES). K_{sp} was calculated using equations 1-3. Stoichiometric ratios were assumed based on the formula from the single crystal structure solution.

$$K_{\mathrm{sp}} = [\mathrm{Ag}^+]^3 \text{ (for CPs SVX and SBX, X = A, N, P, B, R)} \quad \text{Eq. 1}$$

$$K_{\mathrm{sp}} = [Ag^+]^2[0.5Ag^+]^{0.5} \text{ (SBC)} \quad \text{Eq. 2}$$

$$K_{\mathrm{sp}} = [Ag^+][1.25Ag^+]^{1.25}[0.5Ag^+]^{0.5} \text{ (SVC)} \quad \text{Eq. 3}$$

Anion exchange: A typical exchange was 20 mg of CP into 5 mL of 10 mM anion solution forming a 1:1 molar ratio of material to exchange anion. Competing anion solutions were made from $NaClO_4$, $NaNO_3$, $NaCH_3CO_2$, K_2CrO_4, NH_4BF_4 and NH_4ReO_4 salts with pH values of 5.0(5), 5.5(5), 6.0(5), 7.0(5), 5.0(5), and 5.0(5), respectively. A solution of sodium formate was synthesized by titrating formic acid to pH 7 with 1 N NaOH. The CP and anion solutions were allowed to react in the dark for 35 d under static conditions. 0.5 mL aliquots were passed through a 0.45 μm filter and measured on a Dionex Ion Chromatography (IC) system using an isocratic 50 mM NaOH eluent and an IonPac AS20 Analytical Column, AG20 Guard Column and an ADRS 600 suppressor.

Kinetic modeling: The anion exchange data adsorption kinetics were fit to pseudo-second order (PSO) and pseudo-first order (PFO) adsorption models.[66,67] The PFO kinetic adsorption data was plotted as $\ln[q_e - q(t)]$ *vs*. t based on equation 4, where t is time (d), $q(t)$ is mg of anion adsorbed per gram of CP at time t and q_e is $q(t)$ at equilibrium. The rate constant is $k_1 = -m$, where m is the slope. The PSO data was plotted as $\frac{t}{q(t)}$ *vs*. t based on equation 5. The rate constant is defined as $k_2 = m^2 \cdot b^{-1}$, where m is the slope and b is the y-intercept.

$$\ln[q_e - q(t)] = -k_1 t + ln(q_e)$$ (pseudo-first order) .....Eq. 4

$$\frac{t}{q(t)} = \left(\frac{1}{q_e}\right) t + \frac{1}{k_2 q_e^2}$$ (pseudo-second order) .....Eq. 5

Powder X-ray diffraction (PXRD): PXRD experiments were performed on a Rigaku Miniflex X-ray Diffractometer. Powders were analyzed using Cu-Kα 1.5418 Å average radiation wavelength in Bragg-Brentano mode at a rate of 3°/min, step size of 0.02° and range of 2-60° (2θ) on an aluminum sample holder.

In-situ variable-temperature powder X-ray diffraction (VT-PXRD): VT-PXRD experiments were performed on a Rigaku Smartlab X-ray Diffractometer with an Anton Paar DHS 1100 Domed Hot Stage. Powders were analyzed using Cu-Kα 1.5418 Å average radiation wavelength, parallel beam mode at a rate of 3°/min, step size of 0.02° and range of 2-60° (2θ). The diffractometer was set up using 5.0° Soller slit, 0.114° parallel slit analyzer (PSA) and 1 mm, 10 mm, 10 mm for incident slit, receiving slit 1 and receiving slit 2, respectively. Measurements were carried out under flowing nitrogen gas enclosed in the graphite dome. Samples were prepared as compressed films on borosilicate glass slides.

Thermogravimetric analysis (TGA): TGA experiments were performed on a TA Instruments TGA Q500. A finely ground sample was placed in an aluminum pan and heated to 580 °C at 5 °C/min under a continuous flow of nitrogen gas.

Single crystal X-ray diffraction (SCXRD): Crystals of SVB, SVC and SVN were grown as described above. Crystals suitable for SCXRD were selected under a microscope and mounted onto a MiTeGen polyimide sample loop using Type NVH Cargille Immersion Oil. SCXRD experiments were performed on a Rigaku XtaLAB Synergy-S Single-Crystal Diffractometer using Cu-Kα radiation. The structure was solved using SHELXT and refined using SHELXL[68] as implemented in Olex2,[69] following established strategies.[70] All non-H atoms were refined anisotropically. C-bound H atoms were placed at calculated positions and refined with a riding model and coupled isotropic displacement parameters of 1.2 × U_{eq}. O-bound H atoms were located in the Fourier

difference map and refined with chemically reasonable distance restraints and coupled isotropic displacement parameters of 1.5 × U_{eq}. For SVC, isotropic displacement parameters for O-bound H atoms were freely refined. Disordered atoms were treated with similarity and rigid bond restraints. Visualization was performed with Olex2,[69] Mercury[71] and VESTA[72] software packages.

Computational details: All computational work was performed using the open source plane-wave code Quantum ESPRESSO[73] package v6.7. Projector augmented wave (PAW)[74,75] pseudopotentials were used with Perdew-Burke-Ernzerhof (PBE)[76] functionals[77] at wavefunction and charge density cutoffs of 70 and 540 Rydberg (Ry), respectively. Ligand geometries were relaxed in 30 Å cubic boxes at various starting geometries. The detailed procedure and an example input file are provided in the Supporting Information.

Results and Discussion:

Acronyms:

SVX [S = silver, V = Vpe, X = N (nitrate), B (tetrafluoroborate), C (chromate), P (perchlorate), R (perrhenate)]: SBX [S = silver, B = bipy, X = A (acetate), N (nitrate), B (tetrafluoroborate), C (chromate), P (perchlorate), R (perrhenate)].

Synthesis:

Off-white powders of SVB and SVP were synthesized in water at room temperature. Hydrothermal synthesis at 120 °C to 150 °C produced low quality microcrystalline needles. Temperatures above 150 °C produced brown powder with little-to-no crystallinity. Single crystal quality SVB was successfully synthesized by slow evaporation of a mixture of water, methanol, 2-propanol and ammonium hydroxide hexagonal platelets of ~0.2 x 0.2 mm^2 often breaking in half forming trapezoid platelets (Figure S1A). The projected powder pattern from the subsequent SCXRD data (*vide infra*) matches that of the experimental powder pattern (Figure S2). SVP consistently produces fine polycrystalline powders consisting of highly stacked platelets, none of which were of single crystal quality (Figure S1D). SVP is represented consistently in PXRD with distinct reflections (Figure 1). A microcrystalline powder of SVN was synthesized using a mixture of water, 2-propanol and ammonium hydroxide as reported by Khmelevskaya *et al*.[78] PXRD of bulk SVN matches the theoretical pattern. Microcrystalline SVR was synthesized from silver diamine hydroxide and Vpe producing clear needles ~0.3 x 0.02 mm^2 (Figure S1C). The room temperature synthesis product consisted of polycrystalline needles and powder, whereas low temperature synthesis produced high quality colorless crystals. PXRD of the room temperature synthesized powder matches the theoretical PXRD from the single crystal structure (Figure S3).

SVC was synthesized by the same method as SVR, resulting in high quality yellow platelets ~ ~ 0.5 x 0.04 mm^2 (Figure S1B). PXRD of the bulk material matches the theoretical pattern produced from the SCXRD structure (Figure S4). All powders were highly crystalline (Figure 1).

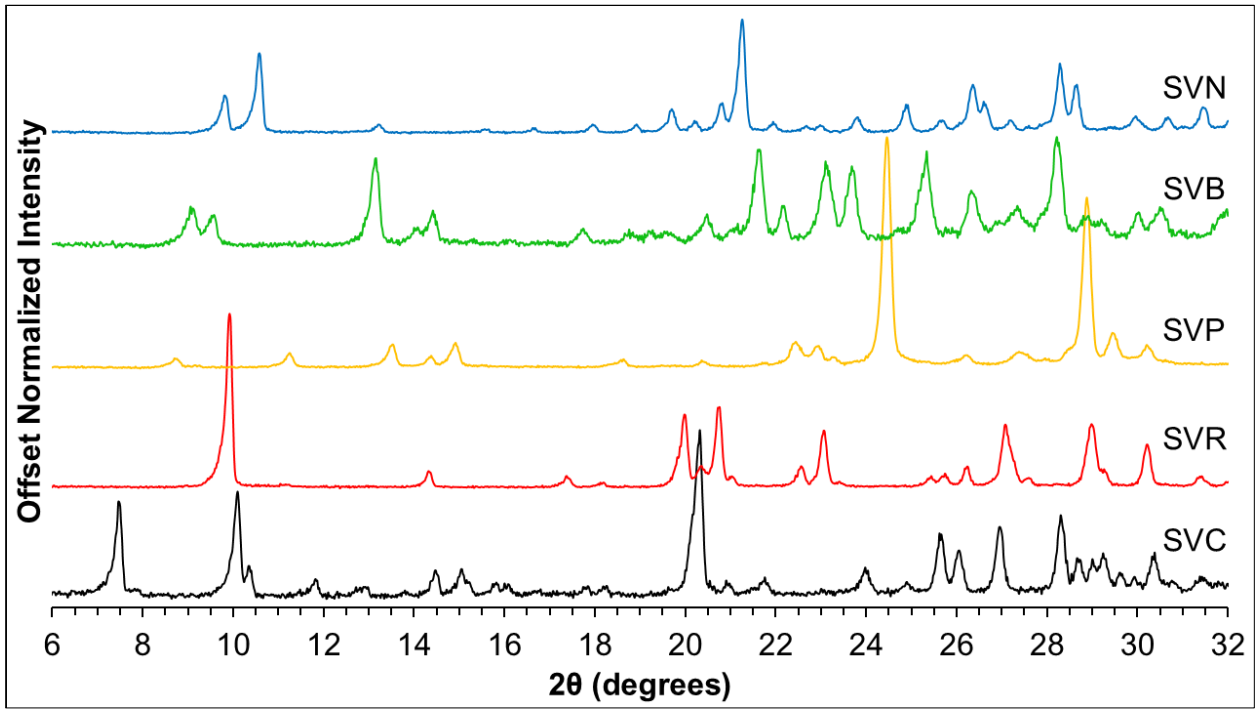

Figure 1. Powder diffraction patterns of synthesized silver Vpe nitrate (SVN), tetrafluoroborate (SVB), perchlorate (SVP), perrhenate (SVR) and chromate (SVC). Patterns normalized to the most intense peak. SVP, SVR and SVC intensity amplified 2x, 1.5x and 1.5x, respectively for clarity.

Single Crystal Structural Characterization:

The structures SVB, SVC and SVR show both heterocyclic nitrogen atoms of the Vpe ligand form μ-2 dative bonding bridging two silver atoms in a linear fashion, forming the $[Ag\text{-}Vpe^+]_n$ polymer (Figures 2 to 4). The same type of linear polymeric connectivity is seen in the bipy structures.[3,9,79–81] The SVB asymmetric unit was determined to contain $[Ag(Vpe)^+][BF_4^-]$ in space group $P\bar{1}$ with $Z = 4$ (Table 1). The Vpe ligand in SVB, as shown in Figure S5, has two equivalent orientations (Figure 2, right). The charge balancing BF_4^- anions are sandwiched between polymer layers near the Ag^+ centers. Pairs of Ag···Ag close contacts are seen, with an average distance of 3.4436(9) Å. Ag^+ and BF_4^- ions form numerous Ag-F close contacts in SVB, from 2.8415(18) to 3.429(3) Å. The $[Ag\text{-}Vpe^+]$ layers alternate orientation perpendicular to the chain axis (Figure 2, left). Both orientations of the polymer chains likely experience strong van der Waals

interactions, often described as π-stacking,[82] with an average distance (plane to plane centroid) of 3.4291(7) Å. The close contact ligand stacking is offset by an average of 1.91(8) Å, forming staircase-type stacking and reducing ligand-ligand (L-L) van der Waals interaction (*vide infra*, Table 2).

Table 1. Crystallographic parameters for SVB, SVC and SVR

Compound	**SVB**	**SVC**	**SVR**
Empirical formula	$C_{12}H_{10}AgBF_4N_2$	$C_{30}H_{35}Ag_2CrN_5O_9$	$C_{12}H_{14}AgN_2O_6Re$
Formula Weight (g/mol)	376.90	877.37	576.32
Temperature (K)	106.66(10)	99.97(17)	100.0(2)
Wavelength (Å)	1.54184	1.54184	1.54184
Crystal system	Triclinic	Triclinic	Monoclinic
Space group	$P\bar{1}$	$P\bar{1}$	$P2_1/m$
***a* (Å)**	9.9054(3)	11.4753(5)	5.02750(10)
***b* (Å)**	10.6979(3)	12.2834(6)	16.8569(3)
***c* (Å)**	13.7005(4)	12.9347(6)	8.79270(10)
α (°)	67.876(3)	65.651(4)	90
β (°)	70.737(3)	79.200(4)	92.757(2)
γ (°)	82.830(2)	78.699(4)	90
Volume (Å^3)	1269.61(7)	1617.21(14)	744.30(2)
Z	4	2	2
ρ_{calc} (g/mL)	1.972	1.802	2.572
Crystal size (mm^3)	0.33 × 0.11 × 0.07	0.21 × 0.04 × 0.03	0.16 × 0.05 × 0.03
θ range (°)	3.660 to 68.236	3.778 to 72.127	5.036 to 68.246
Total reflections	15578	20184	7539
Unique reflections	4641	6281	1404
Parameters	579	454	117
Completeness (%)	99.9	99.8	99.8
R_{int}	0.0467	0.0469	0.0426
R_1 (I > 2σ)	0.0325	0.0331	0.0223
R_1 (all data)	0.0348	0.0374	0.0238
wR_2 (I > 2σ)	0.0844	0.0903	0.0589
wR_2 (all data)	0.0864	0.0935	0.0597
Goodness of fit, *S*	1.028	1.053	1.084

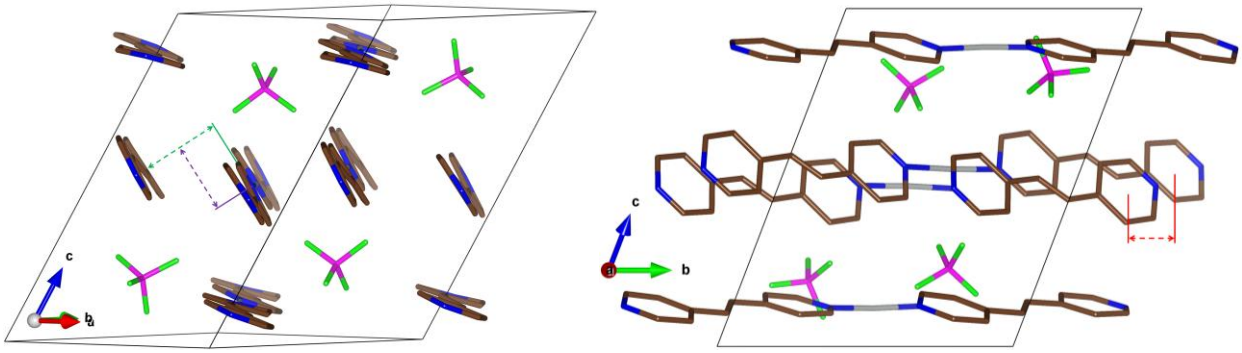

Figure 2. SVB unit cell shown in stick form, emphasizing its polymeric connectivity. H atoms are omitted for clairty. The Vpe ligand has two orientations, each at 50% probability, omitted for clarity. Color code: Ag grey, N blue, C brown, B pink, F green. Green, purple and red dotted lines denote L-L stacking distance, side to side stacking shift and end to end stacking shift, respectively.

SVC {$[Ag_2(Vpe)_{2.5}^{2+}][CrO_4^{2-}]\cdot 5H_2O$, Figures 3 and S6} crystallizes in space group $P\bar{1}$ with $Z = 2$ (Table 1). There are two Ag^+ equivalents in the formula due to the divalent charge of CrO_4^{2-}. Within the unit cell, two silver centers form oxygen-bridged four-membered rings between the two silvers and two chromate ions, with Ag-O bond lengths of 2.582(3) and 2.654(3) Å (Figure 3). The two silver atoms form an argentophilic Ag···Ag close contact of 3.2732(5) Å.[83,84] The chromate-bound silver atoms form a distorted tetrahedral geometry with two Vpe ligands and two chromate oxygen atoms. The remaining two linear ligand-linked silver atoms within the unit cell are isolated from charge balancing chromates. The Ag-N bond lengths do not deviate significantly between the chromate-bound and chromate-unbound silvers. Free Vpe ligands and five water molecules also reside between the Ag-Vpe layers, whereas only anions and solvent molecules are found in the other Vpe and bipy CPs. Strong overlap of the L-L stacking interaction is present, with an average distance of 3.316(16) Å (Figure 3 left) and an average stacking offset of 2.571(15) Å (Figure 3 right).

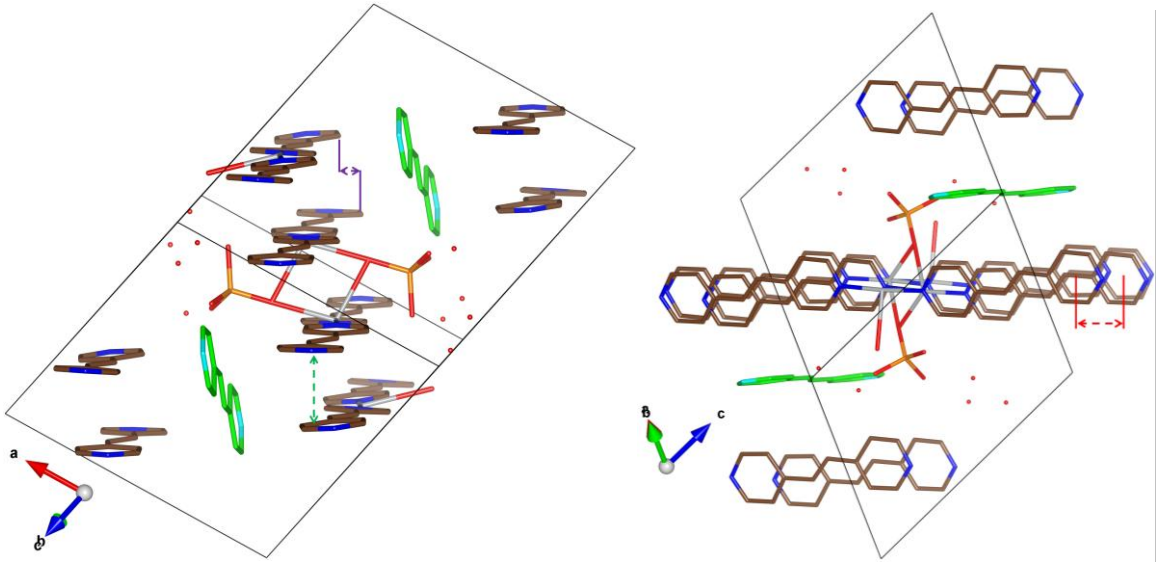

Figure 3. SVC unit cell shown in stick form, emphasizing its polymeric connectivity. H atoms are omitted for clarity. Color code: Ag grey, C brown, N blue, Cr orange, O red. Free Vpe molecules are colored green and light blue for carbon and nitrogen, respectively. Green, purple and red dotted lines denote L-L stacking distance, side to side stacking shift and end to end stacking shift, respectively.

SVR {[Ag(Vpe)$^+$]ReO_4^-]·2H_2O, Figures 4 and S7} crystalizes in space group $P2_1/m$ with *Z* = 2 (Table 1). Vpe and silver coordinating polymer chains form stacked layers along the flat side of the ligand, with interlamellar water and perrhenate. The well-ordered polymer stacking has an average L-L distance of 3.246(3) Å (Figure 4 left). The stacking layers of Vpe are slightly tilted (fold angle) by 8.54(18)° relative to the adjacent ligand stacks, forming a slight rippled effect. Unlike the other CPs reported, no argentophilic close contact is seen, represented by the L-L stacking shift of 3.851(5) Å. The perrhenate anion is situated between two adjacent silver ions, with a Re-Ag distance of 4.2478(8) Å. The oxygen of the perrhenate anion and the silver cation form a close contact of 2.859(3) Å. Silver-anion close contacts were compared to the Cambridge Structural Database[85] (CSD) using the Conquest[86] software. SVR has an Ag-O distance 1.8 times the standard deviation larger than the average of 2.61(16) Å ($n = 40$, where n is the number of structures found in the CSD).

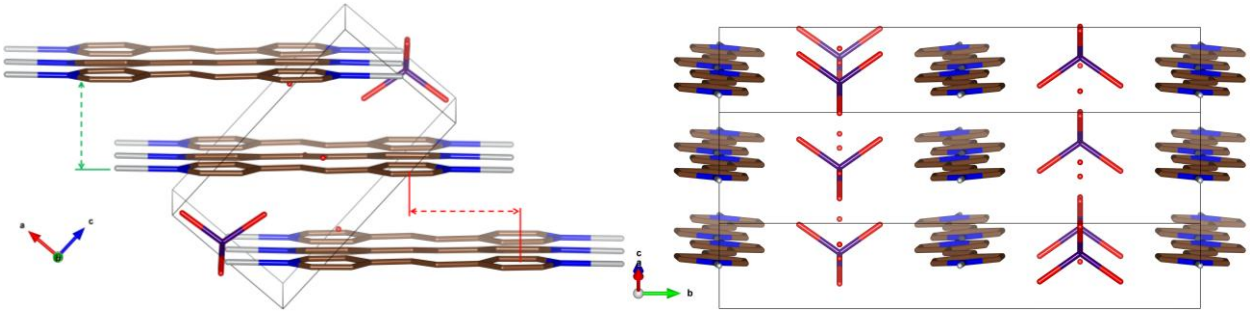

Figure 4. SVR unit cell shown in stick form, emphasizing its polymeric connnectivity. H atoms are omitted for clarity. Color code: Ag grey, C brown, N blue, Re purple, O red. Green and red dotted lines denote L-L stacking distance and end to end stacking shift, respectively.

SVN was reported by Kokunov *et al*.[78] with a CP structure similar to SVB, SVC and SVR, forming $[Ag(Vpe)^{+}][NO_3^{-}]\cdot 3H_2O$ (Figure 5). The Vpe ligands stack with strong overlap and average distance of 3.37(3) Å. Distinct layers of Ag-Vpe polymer stacking with nitrate and water between the layers. No direct Ag-ONO_2 contacts are present within the SVN crystal. Occluded water between the silver and nitrate ions form a hydrogen bonded network, with Ag-OH_2 distances of 2.817(5) Å. The SVP CP structure is as-yet unknown; to date it has only been isolated as low crystallinity powder.

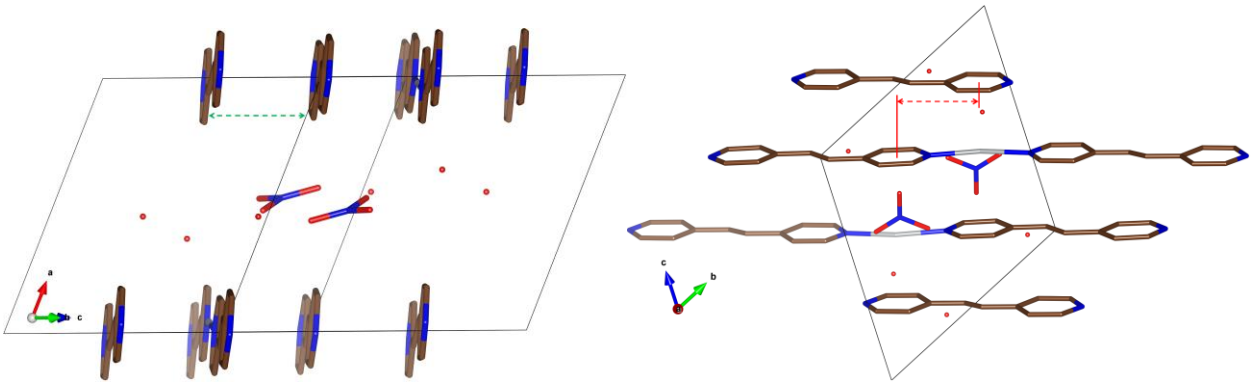

Figure 5. SVN shown in stick form, emphasizing its polymeric connectivity. H atoms are omitted for clarity. Color code: Ag grey, C brown, N blue, O red. Structure images produced from published SVN single crystal data.[78] Green and red dotted lines denote L-L stacking distance and end to end stacking shift, respectively.

Silver-Anion Binding:

SVN, SVB, SVR and SVC display differences in silver-anion binding. SVB has Ag-FBF_3 close contacts ranging from 2.8415(18) to 3.429(3) Å. Ag-F contact distances in Ag-FBF_3 containing structures on average are 2.58(12) Å ($n = 102$). The less specific Ag-F close contact average was 2.55(16) Å ($n = 270$), both values noticeably shorter than that seen in SVB. In the SVC structure, silver and the oxygen of the chromate ion (Ag-$OCrO_3$) form a close contact of 2.582(3) Å, longer but within one standard deviation of the average distance of 2.52(14) Å ($n = 286$). Non-specific Ag-O contacts are typically shorter, with an average distance of 2.45(16) Å ($n = 35{,}856$), while the salt Ag_2CrO_4 has a shorter Ag-O distance of 2.360(17) Å. Ag-$OReO_3$ within the SVR crystal forms close contacts of 2.859(3) Å, 1.8 times the standard deviation larger than the average 2.61(16) Å ($n = 40$) seen on the CSD. SVB, SVC and SVR form longer contacts than most metal-organic complexes and their respective silver salts.[87–89] SVN

is a notable exception, with no direct close contact between the silver and nitrate ions. Similar long contacts are seen in SBX CPs with average contacts of 2.651(4), 2.90(2), 2.88(3), 2.942(2) and 2.603(4) Å for SBA, SBN, SBP, SBR and SBC, respectively. No significant differences are seen in silver-anion binding between SBX and SVX CPs. An imperfect inverse trend of Ag-N bond length relative to the silver-anion contact distance is present. SBA, SBN, SBP, SBR, SBC, SVN, SVB, SVR and SVC have average silver-nitrogen bond lengths of 2.193(4), 2.157(4), 2.151(8), 2.137(2), 2.139(8), 2.124(6), 2.125(6), 2.141(3) and 2.158(4) Å, respectively. It is unclear the impact of silver-anion binding on the overall CP stability, but SBX and SVX CPs show longer contact distances than their respective silver salts[87–92] and complexes from the CSD, suggesting weak coordination.

Computed Ligand Conformation Energetics

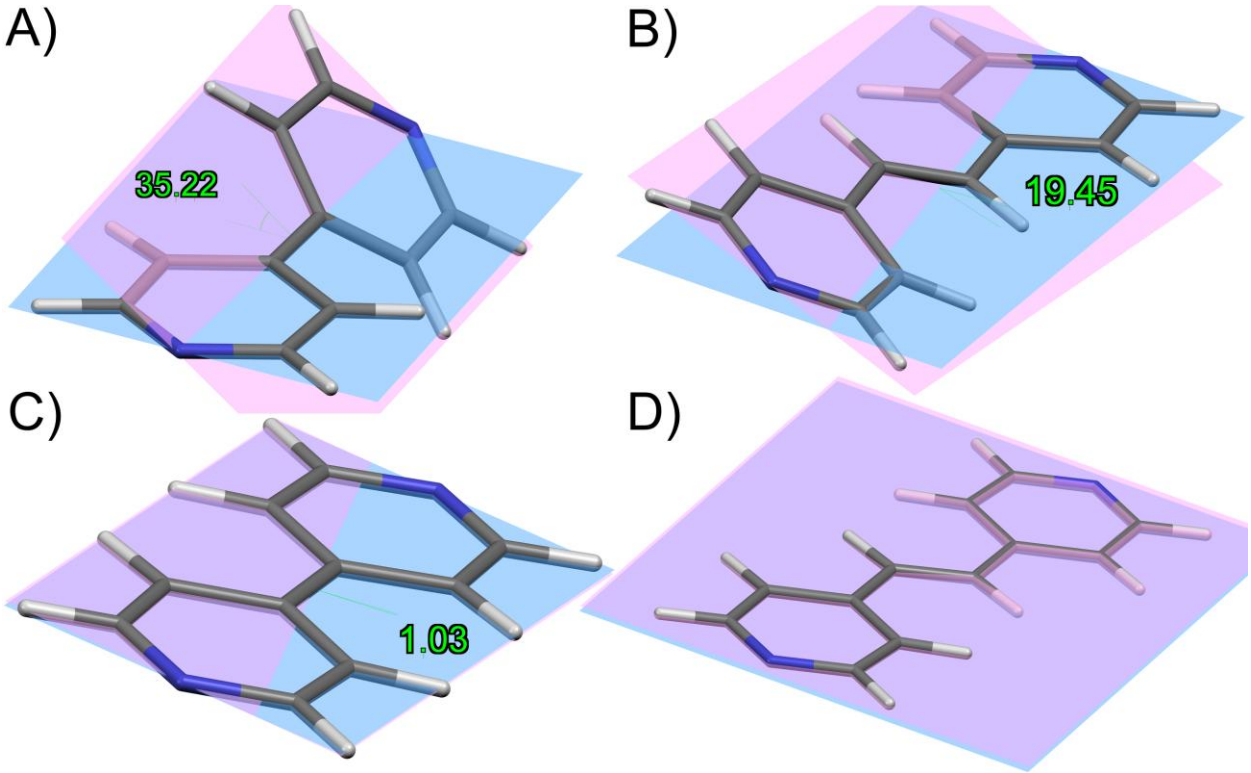

Figure 6. The dihedral angle of the ligand's pyridyl planes after geometry relaxation: A) 4,4′-bipyridine, 35.22°; B) 4,4′-bipyridine, 1.03°; C) 4,4′-vinylenedipyridine, 19.45°; D) 4,4′-vinylenedipyridine, 0.02°.

To better understand the differences between the ligands, total energy calculations were performed on gaseous bipy and Vpe. By varying the starting conformations, relative energies were assigned to flat or torsional twisted geometries. Bipy was geometrically relaxed from a perfectly flat orientation and a gauche orientation (Figure 6). The dihedral angles of all systems were calculated by measuring the angle

between the normal vectors of the planes that best fit each pyridyl unit. The bipy ligand is shown to have a thermodynamically favorable position, with a torsional (~ dihedral) angle of 35.22°, compared to the nearly flat bipy dihedral angle of 1.03°. The 35.22° geometry was calculated to be 5.2 kJ/mol more energetically favorable than the flat geometry, which is in agreement with published results.[93,94] The difference in energy between the two geometries is likely due to the steric effects of the 2, 2′, 6 and 6′ position hydrogen atoms.

The magnitude of the steric effect in Vpe compared to bipy is reduced due to the separation by the carbon-carbon double bond between the pyridine rings, encouraging a flat geometry. Two energetic saddle points were determined for Vpe: a near perfectly flat geometry with a dihedral angle of 0.02° and another with a dihedral angle of 19.45° between the rings. Some torsional stress is spread to the central carbon and hydrogen atoms. The plane that best fits the olefinic carbon and hydrogen atoms form an average torsional angle of 2.88° relative to planes of the pyridyl rings of 2.88° for the flat Vpe (Figure S8). The 19.45° geometry was 0.4 kJ/mol less favorable than the flat geometry. The offloading of the torsional stress through the central atoms could explain the low energy difference between the flat and 19.45° conformations. This is an important distinction when it comes to CPs, as the formation of the crystals tends to induce a geometry change on the ligand and likely comes at an energetic cost.

Table 2. Ligand geometry in coordination polymers

	Torsion Angle (°)	Ligand stacking (Å)	Side to side Stacking	End to end stacking
SVN	0.0(5)	3.380(7)	overlap	overlap
SVB	4.5(11)	3.4291(7)	staircase	overlap
SVC	6.68(17)	3.438(3)	staircase	offset
SVP	--	--	--	--
SVR	0.0(3)	3.246(3)	overlap	offset
Vpe hydrate	20.15(7)	--	staggard	offset
Flat Vpe[a]	0.019	--	--	--
Bent Vpe[a]	19.45	--	--	--
SBA[b]	6.1(2)	3.442(8)	overlap	offset
SBN	0.00	3.328(5)	T-shaped	T-shaped
SBB[c]	18.9(9)	3.413(11)	staggard	staggard
SBC	29.6(2)	3.362(6)	overlap	overlap
SBP	8(1)	3.3875(4)	staggard	staggard
SBR	22.61(7)	3.324(4)	staggard	overlap
Bipy	26.69(13)	--	staggard	staggard
Bipy hydrate	41.63(10)	--	overlap	overlap
Bipy flat[a]	1.03	--	--	--

Bipy bent[a]	35.22	--	--	--

End to end stacking is L-L stacking in the polymer chain (L-Ag-L) direction. Side to side stacking is L-L stacking perpendicular to the polymer chain direction. Overlap denotes nearly no L-L stacking shift. Staircase denotes a significant L-L shift forming a "staircase". Staggard denotes a shift in every other ligand layer. Offset is similar to staircase but instead a shift in the polymer chain direction. Ligand stacking images of 4,4'-bipyridine structures and hydrated 4,4'-vinylenedipyridine can be seen in Figures S9 to S17. Torsion angle and ligand stacking measurements defined in Supplementary Information.

[a]Computationally derived structures

[b]SBA denotes silver 4,4′-bipyridine acetate

[c]SBB structure is not fully refined, therefore distances and angles are used as a general refence only.

Silver CPs tend to alter the ligand geometry, as seen in both bipy and Vpe single crystal data. Solid neat bipy crystals have two conformations, with dihedral angles of 18.50(9)° and 34.87(10)°, for a combined average of 26.69(13)°[59] (Table 2). The hydrated crystal form produces an average dihedral angle of 41.63(10)°.[60] CP formation tends to flatten the 4,4′-bipyridine ligand. SBA, SBN, SBB, SBP, SBR and SBC show average dihedral angles of 6.1(2)°, 0.00°, 18.9(9)°, 8(1)°, 22.61(7)° and 29.6(2)°, respectively. From torsion energetics alone SBC has the most stable confirmation followed by SBR, SBB, SBP, SBA and SBN. All CPs endure a torsion angle reduction cost by flattening the bipy ligand. The average ligand stacking distances are 3.442(8) Å, 3.328(5) Å,[79] 3.413(11) Å, 3.3875(4) Å, 3.324(4) Å,[80] and 3.362(6) Å,[9] respectively which no do directly correlate with the torsion angle. Previous computational studies of gas phase pyridine dimers suggest pyridine ring stacking distances are closer and more energetically favorable when the rings are offset and antiparallel.[95,96] Another study suggests a slight offset with parallel pyridines is also energetically preferred.[97] All the bipy CPs show a staggard or offset L-L stacking improving interactions and likely minimizing L-L distances. Reducing the flattening cost with staggard ligand stacking would likely result in an energetically more favorable crystal structure.

Vpe, a naturally flat bipyridine-like ligand, is an excellent candidate for studying the impact of ligand torsion on 1D silver CPs. The hydrated crystal form of Vpe displays a dihedral angle of 20.15(7)°.The occluded water induces higher dihedral angles in both Vpe and bipy (Table 2). The average dihedral angles of SVR, SVN, SVB and SVC are 0.0(3)°, 0.0(5)°, 4.5(11)° and 6.68(17)°, respectively, which correlate with the average ligand stacking distances of 3.246(3) Å, 3.380(7) Å, 3.4291(7) Å and 3.438(3) Å, respectively. SVR and SVN keep the flat geometry while for SVB and SVC, an induced torsional twist is seen. This torsional conformation imposed on the Vpe ligand seems to be accompanied by a ligand stacking offset arrangement as compared to SVN and SVR (Figures 2 to 5). SVC shows an induced torsion in the Vpe ligand significantly higher than the other CPs, but that cost is likely under 0.4 kJ/mol as suggested by the gas phase ligand calculations and accompanied by end to end and side to side displacements. While induced geometry is seen in both Vpe and bipy CPs, the

energetic cost is significantly reduced with Vpe by as high as 4.8 kJ/mol. The crystal energetics are impacted by many factors, especially when it comes to crystal geometry and packing for which simple observational trends are inadequate. The torsional strain is nevertheless an important contribution to the total crystal energetics. The rigid yet energetically flexible Vpe ligand clearly reduces overall formation energies and increases aqueous stability over bipy CPs.

Anion Exchange

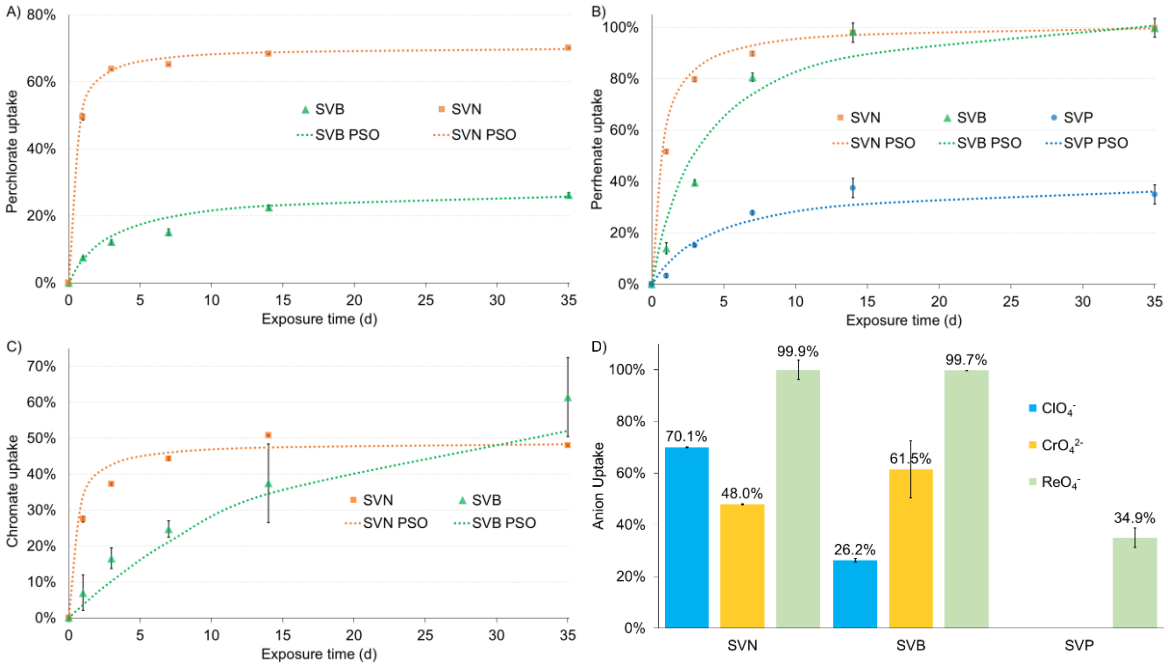

Figure 7. Anion uptake of (A) perchlorate, (B) perrhenate and (C) chromate over 35 d static exchange; (D) final anion uptake values. Anion exchange was performed in 1:1 molar ratio and ~ 260:1 liquid to CP mass ratio, with pH-unadjusted anion solutions of 5.0(5), 5.0(5) and 7.0(5) for $NaClO_4$, NH_4ReO_4 and K_2CrO_4 solutions, respectively. Solid markers are the experimental uptake, and dotted lines are calculated from the kinetic model. The reported values are the average of three independent experiments and the reported uncertainty is equal to one standard deviation. Error bars not easily visible are hidden by data point marker.

Coordination polymers SVN, SVB and SVP were exposed to equimolar anion solutions of formate, acetate, nitrate, perchlorate, perrhenate and chromate for two weeks. These specific anions were examined for direct comparison to previous work on SBX CPs to elucidate ligand effects. The exchange was performed under static conditions to slow the exchange kinetics. Uptake percentages were determined *via* ion chromatography (Figure 7). All materials were unable to take up formate or acetate anions, with formate concentration remaining constant and only a few percent of acetate

adsorbed after exposure (Figure S18). The divalent charge of chromate forms a CP with at least twice the molar requirements of the silver and ligand per formula unit than the other CPs. A 50% uptake is thus equivalent to complete transformation to the chromate CP, releasing two monovalent anions for every chromate sequestered.

SVN exhibited a preference for perrhenate at nearly complete uptake [100(4)%, 620(2) mg/g], followed by chromate [48.0(2)% (of 50% theoretical capacity), 136.1(6) mg/g] and perchlorate (70.1(2)%, 171.6(4) mg/g). SVB also reached near complete exchange of perrhenate (99.96(4)%, 661.8(3) mg/g), followed by chromate (61(11)%, 190(3) mg/g), perchlorate (26.2(7)%, 69(2) mg/g) and negligible nitrate adsorption. The chromate exchange using SVB exceeded the theoretical limit of 50%, with a very high uncertainty of 11%, likely due to an unknown degradation mechanism with the SVB CP. SVP displayed negligible uptake for all anions except for perrhenate at 35(4)%, 220(2) mg/g. The coordination polymers exhibited a preferred exchange order of R > P > C, suggesting a thermodynamic hierarchy conserved in the tested CPs. The static conditions greatly reduced adsorption rates but thermodynamic equilibrium was likely reached.[98,99] With the introduction of stirring, SVN after 3 d sequestered perrhenate (99.8%) and chromate (46.4%). Stirring thus achieved a degree of exchange roughly equal to static conditions and can thus also be considered to have reached thermodynamic equilibrium.

Table 3. Kinetic data: Pseudo-second order and pseudo-first order rate constant (k_2), absorption capacity at equilibrium (q_e) and coefficient of determination (R^2) for the exchange reactions

	Pseudo-Second Order (PSO)			Pseudo-First Order (PFO)			
exchange reaction	k_2	q_e	R^2	k_1	q_e	R^2	q_e (Exp)
$SVN + ClO_4^- \rightarrow SVP$	0.01671	177.0	0.99976	0.2200	72.12	0.78840	175.9
$SVB + ClO_4^- \rightarrow SVP$	0.004672	71.38	0.97881	0.1288	59.90	0.97076	67.10
$SVN + ReO_4^- \rightarrow SVR$	0.002389	653.6	0.99926	0.2636	430.4	0.96314	642.6
$SVB + ReO_4^- \rightarrow SVR$	0.0003894	740.7	0.96528	0.3167	850.8	0.98134	666.4
$SVP + ReO_4^- \rightarrow SVR$	0.0008685	261.1	0.91580	0.01159	569.8	0.58525	224.6
$SVN + CrO_4^{2-} \rightarrow SVC$	0.03058	73.10	0.99819	0.3409	53.53	0.94959	71.62
$SVB + CrO_4^{2-} \rightarrow SVC$	0.001119	106.0	0.87810	0.06450	86.41	0.98576	91.38

Data derived from equations 4 and 5. $q_e = g(CP) \cdot mg^{-1}(Anion), k = q_e \cdot t^{-1}$

Anion adsorption kinetics were fit to pseudo-second order and pseudo-first order adsorption models (Table 3).[66,67] To better correlate the kinetic models with experimental exchange, the models were graphed as dotted lines in Figure 7. As seen in Table 3, SVN and SVP data matches PSO, with high R^2 and similar q_e values. SVB adsorption of ClO_4^- also more strongly correlates to PSO, with a higher R^2 (0.97881) and predicts q_e more accurately. For SVB adsorption of ReO_4^-, however, PSO has a

lower R^2 than PFO but predicts q_e more accurately than PFO. SVB adsorption of CrO_4^{2-} matches PFO, with a higher R^2 of 0.98576 and predicts the q_e comparably to PSO. PSO kinetics better match the ion exchange reactions of SVN, SVB and SVP than PFO in the prediction of q_e. Apart from SVB, the anion exchange reactions show stronger correlation to PSO over PFO with higher R^2 values.

Thermodynamics

Table 4. Coordination Polymer Solubility. Aqueous solubility of silver bipy and silver Vpe coordination polymers derived from silver concentration determined by ICP-OES. Values are based on the assumption that one silver species is representative of the dissolution of one formula unit.

CP	[Ag^+] (mM) = CP solubility	CP Solubility (g/L)	K_{sp}	ΔG_f[a] (kJ/mol)
SVN	0.181(3)	0.0737(11)	6.0(3) x 10^{-12}	–64.03(11)
SVB	0.21(5)	0.080(19)	1.1(6) x 10^{-11}	–63.0(18)
SVP	0.0397(14)	0.0159(5)	6.3(6) x 10^{-14}	–75.3(3)
SVR	0.0137(7)	0.0079(4)	2.6(4) x 10^{-15}	–83.2(4)
SVC	0.049(3)	0.043(3)	1.3(2) x 10^{-12} [b]	–67.8(4)[b]
SBA	5.5(5)	2.1(2)	1.7(4) x 10^{-07}	–38.7(6)
SBN	0.973(7)	0.317(2)	9.2(2) x 10^{-10}	–51.57(5)
SBB	0.812(9)	0.299(3)	5.3(2) x 10^{-10}	–52.92(8)
SBP	0.227(3)	0.0854(13)	1.18(5) x 10^{-11}	–62.38(11)
SBR	0.045(3)	0.0232(16)	9.3(18) x 10^{-14}	–74.4(5)
SBC[9]	0.1578	0.122	2.21 x 10^{-10} [b]	–55.[b]
AgCl[100]	n/a	n/a	1.8 x 10^{-10}	–56

K_{sp} values for CPs were calculated from Equations 1-3.

[a] $\Delta G_f = -\Delta G_{solution} = RTln(K_{sp})$, *where* $T = 298\ K$, $R = 0.008314\ kJ{\cdot}mol^{-1}{\cdot}K^{-1}$

The reported values are the average of three independent experiments and the reported uncertainty is equal to one standard deviation. Independent experiments for SVB and SVP were five and four, respectively.

[b] *SVC and SBC K_{sp} and ΔG_f are derived from molecular formulas with one silver.*

Dissolution reaction: $\mathrm{SVX(s)} \rightleftharpoons \mathrm{Ag^+(aq) + Vpe(aq) + X^-(aq)}$.....Eq. 6

SVX CPs were submerged in water for 7 d to reach their solubility equilibrium following Eq. 6. The silver ion concentration of the supernatant was measured by ICP-OES and used to extrapolate their respective solubility and ΔG_f (Table 4). The molar solubility of silver Vpe anion CPs was significantly less than that of silver bipy anion CPs by a factor of 3.2 to 5.7. Although the solubility order of SVX is consistent with that of the SBX CPs, the impact of each anion varies. The molar solubility of SVX CPs shows a preferred anion trend of R > P > C > N > B, which is similar to the SBX CP trend of R >

P > C > B > N > A. The SVX solubility trend matches that seen in the anion exchange data (Figure 7) for SVR and SVP. The ability of SVN and SVB to adsorb chromate deviates from expectation based on solubility alone. The deviation is likely a consequence of equimolar exchange replacing two anions per chromate encouraging SVC formation. Despite the 2:1 anion exchange, the facile conversion of SVP to SVC is consistent with the solubility data. The SVN solubility of 0.181(3) mM is greatly reduced from the SBN solubility of 0.973(7) mM. SVP, SVR and SVC are also significantly less soluble than their bipy equivalents by 5.7, 3.3 and 3.2 times, respectively.

Clearly, the minor structural change in the ligand significantly impacts the overall solubility of the CPs. Vpe is of larger size and its nonpolar double bond enhances conjugation, promoting a flat geometry conducive to π–π stacking and greater van der Waals interaction. SVX CPs on average have a more favorable ΔG_f of 11.5 kJ/mol than SBX CPs. The difference in ΔG_f likely comes from the 4.8 kJ/mol maximum torsional energy reduction along with increased van der Waals interactions estimated to be 5 –10 kJ/mol[101] for L-L stacking. This increase in aqueous thermodynamic stability is important for sequestering the desired pollutant in the presence of competitive ions such as chloride, which can form insoluble silver chloride.

Table 5. Reaction free energy of anion exchange. Green indicates a spontaneous uptake of anion by the CP starting material, orange indicates an unfavorable reaction.

Starting Material	Anion exchange reaction ΔG (kJ/mol)					
	$CH_3CO_2^-$	BF_4^-	NO_3^-	CrO_4^{2-}	ClO_4^-	ReO_4^-
SVB		--	-1.0	-4.8	-12.3	-20.2
SVN		1.0	--	-3.8	-11.3	-19.2
SVC		4.8	3.8	--	-7.5	-15.4
SVP		12.3	11.3	7.5	--	-7.9
SVR		20.2	19.2	15.4	7.9	--
SBA	--	-14.2	-12.9	-16.4	-23.7	-35.7
SBN	12.9	-1.3	--	-3.5	-10.8	-22.8
SBB	14.2	--	1.3	-2.2	-9.5	-21.4
SBC	16.4	2.2	3.5	--	-7.3	-19.3
SBP	23.7	9.5	10.8	7.3	--	-12.0
SBR	35.7	21.4	22.8	19.3	12.0	--

The anion exchange reaction free energy is $\Delta G_{Exch} = \Delta G_{f,product} - \Delta G_{f,reactant}$. The exchange reaction with equimolar anion concentrations: $SVY(s) + X^-(aq) \rightarrow SVX(s) + Y^-(aq)$, where X is the anion adsorbed and Y is the anion released. Chromate exchange reaction free energies are calculated with two exchanged anions per chromate.

The solubility data indicates that silver Vpe CPs could reduce target anion concentrations more effectively than their bipy counterparts. At solubility equilibrium

concentrations, anions are also released and can be used as indicators for concentration reduction limits. The ion exchange reaction free energy seen in Table 5 suggests exchange order of SVR > SVP > SVC > SVN > SVB. The free energy of exchange suggests SVN and SVB should reach a near complete anion exchange with perrhenate, forming SVR with a ΔG_{Exch} of -19.2 and -20.0 kJ/mol, respectively. From the exchange ΔG_{Exch} constants, k predicts >99.9% exchange, in agreement with the exchange data. Not all the exchanges, however, reached the theoretical value suggested by their free energy values or reaction constants. For instance, the conversion of SVN to SVP is theoretically predicted to reach 99.0% but experimentally reached 70.1%. SVN and SVB reached nearly complete exchange despite ΔG_{Exch} predicts 82.2 and 87.3%, respectively. The expected reaction exchange constants assume ideal behavior, equimolar anion exchange and activity coefficients equal to one. The deviation from ideality is likely due to high concentrations of the releasing ion giving rise to the diverse-ion effect, also known as the uncommon ion effect or the salt effect.[102,103] The ionic strength of the solution and activity coefficients of the solvated species are altered when ions not in the product are present, resulting in higher solubility than K_{sp} would predict. Variation in unlike ion concentration modifies each CPs solubility to a different degree and therefore each anion exchange reaction. Further study is needed to obtain a CP that can reduce anionic pollutants to their maximum contaminant level (MCL). This underscores the necessity of new insights into the ion exchange materials that could allow a rational design approach.

Thermal Stability Investigation

The thermal decomposition of all five CPs was measured using TGA from room temperature to 580 °C as well as by *in-situ* VT-PXRD (Figures S19 to S28). Metallic silver remains after decomposition of all CPs, as indicated by the (111) and (200) reflections at 38.1° and 44.3° (2θ), respectively (asterisks; COD# 9013045).[104] At higher temperature, the 38.1° and 44.3° (2θ) reflections shift slightly to 37.7° and 43.8° (2θ), respectively.

The TGA of SVN (Figure S19) displays two mass loss steps by 95 °C, corresponding to the three occluded waters (experimental, 13.2%; theoretical, 13.3%). The last four decomposition steps by 323 °C likely correspond to the loss of the Vpe ligand and nitrate (experimental, 59.6%; theoretical, 60.1%). VT-PXRD (Figure S20) shows an unknown phase appearing at 150 °C until complete degradation to metallic silver by 350 °C.

SVB (Figure S21) shows a single step decomposition from 225 °C to 380 °C, corresponding to the Vpe ligand and tetrafluoroborate ion (experimental, 70.1%; theoretical 71.4%). VT-PXRD (Figure S22) is consistent, with SVB present at 225 °C

and thermal shifting of reflections to lower angle, indicating unit cell expansion. After decomposition, only metallic silver is present at 400 °C.

SVP (Figure S23) shows a single step decomposition step from 300 °C to 400 °C, corresponding to the loss of more mass than Vpe ligand and perchlorate ion (experimental, 93.0%; theoretical, 72.3%). VT-PXRD (Figure S24) shows thermal shifting of reflections at 300 °C, with reflections at 27.4°, 31.7° and 45.5° (2θ) at 400 °C, indicating the formation of AgCl[105] and a weak metallic silver reflection 37.7° (2θ) at 500 °C. The latter indicates loss of the metallic silver likely due to a redox reaction between the ligand and perchlorate ion.

SVR TGA (Figure S25) shows a loss corresponding to the two occluded waters by 220 °C (experimental, 6.5%; theoretical, 6.3%). 300 °C to 440 °C shows a loss of the Vpe ligand (experimental, 31.6%; theoretical, 31.6%). VT-PXRD (Figure S26) at 200 °C and 250 °C show an unknown material, with traces of metallic silver and rhenium. The weakly diffracting rhenium peak at 39.6° (2θ) matches the theoretical Re (111) reflection, as indicated by a black diamond (Figure S16; COD# 1534939).[106] The final loss at 500 °C (12.7%) is unidentified, though the decomposition residue mass is greater than metallic Ag (experimental, 49.7%; theoretical 18.7%). PXRD at 410 °C and 550 °C shows only metallic silver reflections.

SVC TGA (Figure S27) shows two mass loss transitions before 125 °C, corresponding to the five occluded waters (experimental, 10.3%; theoretical, 10.3%). At 125 °C, the CP transitioned into an unknown phase, as indicated by VT-XRD (Figure S28). The last three decomposition products correspond to ligand loss (experimental, 55.1%; theoretical 51.9%). The final residue at 400 °C shows disordered metallic silver, with extra mass loss (experimental, 34.6%, theoretical 24.6%) likely from the incorporation of chromium and oxygen with the silver, forming a highly disordered solid likely of molecular formula Ag_2CrO_2 (experimental 34.6%; theoretical 34.2%).

Vpe ligand CPs compared to bipy CPs display thermal decomposition temperatures similar to those previously reported.[9,26] Small changes to the ligand or the anion have only minimal effects. Structural water molecules of all CPs tend to be lost at lower temperatures and form unknown phases. SVB and SVP don't show any low temperature transitions and their VT-PXRD suggests the CPs hold their structure to higher temperatures. The Vpe ligand orientations and ligand overlap don't appear to correlate with the thermal stability suggested by the TGA and VT-XRD. This observation suggests structural waters are the dominant factor for temperature sensitivity of the CPs.

Conclusions:

Silver 4,4′-vinylenedipyridine based CPs readily exchange their anions and form highly stable products. Most notably, nitrate and tetrafluoroborate exchange quantitatively for perrhenate, perchlorate and chromate. ΔG_f values suggest an exchange order of SVR > SVP > SVC > SVN > SVB. Equimolar anion exchange experiments show an exchange hierarchy of SVR > SVC ≈ SVP. SVN and SVB adsorbed nearly 100% of both chromate and perrhenate, following PSO kinetics. Comparing the bipy CPs, the Vpe ligand reduces the CP solubility by a factor of 3.2 to 5.7 and therefore increases their stability when in contact with aqueous solutions. This increased stability likely arises from the increased van der Waals forces and conformational energetic cost reduction due to the more rigid Vpe ligand. These results suggest ligands with flat geometries or greater van der Waals interactions are excellent options for stabilizing CPs that are in contact with aqueous solutions. In turn, this approach could give rise to new materials with further improved pollutant trapping properties.

Supporting Information:

Crystallographic structure files for SVB, SVR and SVC (CIF). Additional data and information: thermal ellipsoid figures, crystallographic figures, theoretical PXRD patterns, TGA plots, VT-PXRD patterns, computational details and example input file.

Accession Codes

CCDC 2336941, 2378801 and 2336942 for SVB, SVR and SVC, respectively contain the supplementary crystallographic data for this paper. These data can be obtained free of charge via www.ccdc.cam.ac.uk/data_request/cif, or by emailing data_request@ccdc.cam.ac.uk, or by contacting The Cambridge Crystallographic Data Centre, 12 Union Road, Cambridge CB2 1EZ, UK; fax: +44 1223 336033.

Acknowledgements:

This work was supported in part by the National Science Foundation under grant No. 2044692. The single-crystal X-ray diffractometer housed in the UCSC X-ray Diffraction Facility was funded by NSF MRI grant 2018501. We acknowledge Professor Timothy C. Johnstone and Dr. Daniel G. Droege of the UC Santa Cruz Department of Chemistry & Biochemistry and the X-ray Facility for SCXRD data collection. We also thank Dr. Brian Dreyer from the UC Santa Cruz Plasma Analytical Laboratory, RRID:SCR_021925, for help with elemental analyses.

References:

(1) Colinas, I. R.; Silva, R. C.; Oliver, S. R. J. Reversible, Selective Trapping of Perchlorate from Water in Record Capacity by a Cationic Metal–Organic Framework. *Environ. Sci. Technol.* **2016**, *50* (4), 1949–1954. https://doi.org/10.1021/acs.est.5b03455.
(2) Colinas, I. R.; Inglis, K. K.; Blanc, F.; Oliver, S. R. J. Anion Exchange Dynamics in the Capture of Perchlorate by a Cationic Ag-Based MOF. *Dalton Trans.* **2017**, *46* (16), 5320–5325. https://doi.org/10.1039/C7DT00475C.
(3) Citrak, S. C.; Popple, D.; Delgado-Cunningham, K.; Tabler, K.; Bdeir, K.; Oliver, A. G.; Kvam, P. B.; Oliver, S. R. J. Extremely Rapid Uptake of Perchlorate with Release of an Environmentally Benign Anion: Silver Bipyridine Acetate. *Cryst. Growth Des.* **2018**, *18* (3), 1891–1895. https://doi.org/10.1021/acs.cgd.7b01797.
(4) Srinivasan, A.; Viraraghavan, T. Perchlorate: Health Effects and Technologies for Its Removal from Water Resources. *Int. J. Environ. Res. Public. Health* **2009**, *6* (4), 1418–1442. https://doi.org/10.3390/ijerph6041418.
(5) Gu, B.; Brown, G. M.; Chiang, C.-C. Treatment of Perchlorate-Contaminated Groundwater Using Highly Selective, Regenerable Ion-Exchange Technologies. *Environ. Sci. Technol.* **2007**, *41* (17), 6277–6282. https://doi.org/10.1021/es0706910.
(6) Gu, B.; Brown, G. M.; Alexandratos, S. D.; Ober, R.; Dale, J. A.; Plant, S. Efficient Treatment of Perchlorate (ClO4−)-Contaminated Groundwater with Bifunctional Anion Exchange Resins. In *Perchlorate in the Environment*; Urbansky, E. T., Ed.; Springer US: Boston, MA, 2000; pp 165–176. https://doi.org/10.1007/978-1-4615-4303-9_16.
(7) Roy, S.; Titi, H. M.; Tripuramallu, B. K.; Bhunia, N.; Verma, R.; Goldberg, I. Silver Coordination Polymers Based on Newly Designed Bis(Cyanobenzyl)Bipiperidine Ligand: Synthesis, Anion Exchange, Guest Inclusion, Electrochemical, and Photoluminescence Properties. *Cryst. Growth Des.* **2016**, *16* (5), 2814–2825. https://doi.org/10.1021/acs.cgd.6b00151.
(8) Li, C.-P.; Zhou, H.; Mu, Y.-H.; Guo, W.; Yan, Y.; Du, M. Structural Transformations Induced by Selective and Irreversible Anion Exchanges for a Layered Ag(I) Nitrite Coordination Polymer. *Cryst. Growth Des.* **2017**, *17* (4), 2024–2033. https://doi.org/10.1021/acs.cgd.7b00020.
(9) Conour, C. S.; Droege, D. G.; Ehlke, B.; Johnstone, T. C.; Oliver, S. R. J. Selective Chromium(VI) Trapping by an Acetate-Releasing Coordination Polymer. *Inorg. Chem.* **2022**, *61* (51), 20824–20833. https://doi.org/10.1021/acs.inorgchem.2c03110.
(10) Fei, H.; Han, C. S.; Robins, J. C.; Oliver, S. R. J. A Cationic Metal–Organic Solid Solution Based on Co(II) and Zn(II) for Chromate Trapping. *Chem. Mater.* **2013**, *25* (5), 647–652. https://doi.org/10.1021/cm302585r.
(11) Zhu, L.; Xiao, C.; Dai, X.; Li, J.; Gui, D.; Sheng, D.; Chen, L.; Zhou, R.; Chai, Z.; Albrecht-Schmitt, T. E.; Wang, S. Exceptional Perrhenate/Pertechnetate Uptake and Subsequent Immobilization by a Low-Dimensional Cationic Coordination Polymer: Overcoming the Hofmeister Bias Selectivity. *Environ. Sci. Technol. Lett.* **2017**, *4* (7), 316–322. https://doi.org/10.1021/acs.estlett.7b00165.
(12) Cao, R.; McCarthy, B. D.; Lippard, S. J. Immobilization, Trapping, and Anion Exchange of Perrhenate Ion Using Copper-Based Tripodal Complexes. *Inorg. Chem.* **2011**, *50* (19), 9499–9507. https://doi.org/10.1021/ic201172r.
(13) Ehlke, B.; Conour, C. S.; Vandiver, T. J.; Lofgren, K. C.; Barnett, J. L.; Reinheimer, E. W.; Wenger, J. S.; Oliver, S. R. J. Silver 2,4'-Bipyridine Coordination Polymer for the High-Capacity Trapping of Perrhenate, A Pertechnetate Surrogate. *Inorg. Chem.* **2024**, *63* (19), 8674–8684. https://doi.org/10.1021/acs.inorgchem.4c00202.
(14) Li, J.; Zhu, L.; Xiao, C.; Chen, L.; Chai, Z.; Wang, S. Efficient Uptake of Perrhenate/Pertechnenate from Aqueous Solutions by the Bifunctional Anion-Exchange Resin. *Radiochim. Acta* **2018**, *106* (7), 581–591. https://doi.org/10.1515/ract-2017-2829.

(15) Li, C.-P.; Zhou, H.; Chen, J.; Wang, J.-J.; Du, M.; Zhou, W. A Highly Efficient Coordination Polymer for Selective Trapping and Sensing of Perrhenate/Pertechnetate. *ACS Appl. Mater. Interfaces* **2020**, *12* (13), 15246–15254. https://doi.org/10.1021/acsami.0c00775.
(16) Li, J.; Dai, X.; Zhu, L.; Xu, C.; Zhang, D.; Silver, M. A.; Li, P.; Chen, L.; Li, Y.; Zuo, D.; Zhang, H.; Xiao, C.; Chen, J.; Diwu, J.; Farha, O. K.; Albrecht-Schmitt, T. E.; Chai, Z.; Wang, S. 99TcO4− Remediation by a Cationic Polymeric Network. *Nat. Commun.* **2018**, *9* (1), 3007. https://doi.org/10.1038/s41467-018-05380-5.
(17) Shen, N.; Yang, Z.; Liu, S.; Dai, X.; Xiao, C.; Taylor-Pashow, K.; Li, D.; Yang, C.; Li, J.; Zhang, Y.; Zhang, M.; Zhou, R.; Chai, Z.; Wang, S. 99TcO4− Removal from Legacy Defense Nuclear Waste by an Alkaline-Stable 2D Cationic Metal Organic Framework. *Nat. Commun.* **2020**, *11* (1), 5571. https://doi.org/10.1038/s41467-020-19374-9.
(18) Li, J.; Li, B.; Shen, N.; Chen, L.; Guo, Q.; Chen, L.; He, L.; Dai, X.; Chai, Z.; Wang, S. Task-Specific Tailored Cationic Polymeric Network with High Base-Resistance for Unprecedented 99TcO4– Cleanup from Alkaline Nuclear Waste. *ACS Cent. Sci.* **2021**, *7* (8), 1441–1450. https://doi.org/10.1021/acscentsci.1c00847.
(19) *Activity Coefficients in Electrolyte Solutions*, 2. ed.; Pitzer, K. S., Pitzer, K. S., Chemical Rubber Company, Eds.; CRC Press: Boca Raton, 1991.
(20) Alexandratos, S. D. Ion-Exchange Resins: A Retrospective from Industrial and Engineering Chemistry Research. *Ind. Eng. Chem. Res.* **2009**, *48* (1), 388–398. https://doi.org/10.1021/ie801242v.
(21) Barbaro, P.; Liguori, F. Ion Exchange Resins: Catalyst Recovery and Recycle. *Chem. Rev.* **2009**, *109* (2), 515–529. https://doi.org/10.1021/cr800404j.
(22) Fei, H.; Rogow, D. L.; Oliver, S. R. J. Reversible Anion Exchange and Catalytic Properties of Two Cationic Metal–Organic Frameworks Based on Cu(I) and Ag(I). *J. Am. Chem. Soc.* **2010**, *132* (20), 7202–7209. https://doi.org/10.1021/ja102134c.
(23) Fei, H.; Bresler, M. R.; Oliver, S. R. J. A New Paradigm for Anion Trapping in High Capacity and Selectivity: Crystal-to-Crystal Transformation of Cationic Materials. *J. Am. Chem. Soc.* **2011**, *133* (29), 11110–11113. https://doi.org/10.1021/ja204577p.
(24) Zhang, S.-S.; Wang, X.; Su, H.-F.; Feng, L.; Wang, Z.; Ding, W.-Q.; Blatov, V. A.; Kurmoo, M.; Tung, C.-H.; Sun, D.; Zheng, L.-S. A Water-Stable Cl@Ag14 Cluster Based Metal–Organic Open Framework for Dichromate Trapping and Bacterial Inhibition. *Inorg. Chem.* **2017**, *56* (19), 11891–11899. https://doi.org/10.1021/acs.inorgchem.7b01879.
(25) Nath, K.; Maity, K.; Biradha, K. Two-Dimensional Coordination Polymers with “X”-Shaped Cavities as Adsorbents of Oxoanion Pollutants and Toxic Dyes. *Cryst. Growth Des.* **2017**, *17* (8), 4437–4444. https://doi.org/10.1021/acs.cgd.7b00771.
(26) Citrak, S. C.; Bdeir, K.; Delgado-Cunningham, K.; Popple, D.; Oliver, S. R. J. Exchange Capability of Cationic Silver 4,4′-Bipyrdine Materials for Potential Water Remediation: Structure, Stability, and Anion Exchange Properties. *Inorg. Chem.* **2019**, *58* (11), 7189–7199. https://doi.org/10.1021/acs.inorgchem.9b00115.
(27) Li, J. Q.; Gong, L. L.; Feng, X. F.; Zhang, L.; Wu, H. Q.; Yan, C. S.; Xiong, Y. Y.; Gao, H. Y.; Luo, F. Direct Extraction of U(VI) from Alkaline Solution and Seawater via Anion Exchange by Metal-Organic Framework. *Chem. Eng. J.* **2017**, *316*, 154–159. https://doi.org/10.1016/j.cej.2017.01.046.
(28) Desai, A. V.; Roy, A.; Samanta, P.; Manna, B.; Ghosh, S. K. Base-Resistant Ionic Metal-Organic Framework as a Porous Ion-Exchange Sorbent. *iScience* **2018**, *3*, 21–30. https://doi.org/10.1016/j.isci.2018.04.004.
(29) Lv, L.; Yang, J.; Zhang, H.-M.; Liu, Y.-Y.; Ma, J.-F. Metal-Ion Exchange, Small-Molecule Sensing, Selective Dye Adsorption, and Reversible Iodine Uptake of Three Coordination Polymers Constructed by a New Resorcin[4]Arene-Based Tetracarboxylate. *Inorg. Chem.* **2015**, *54* (4), 1744–1755. https://doi.org/10.1021/ic502686b.

(30) Zhang, Z.; Yang, Y.; Sun, H.; Cao, R. Syntheses, Structures and Anion Exchange Properties of Accommodative Silver Chains Using a Positively Charged and Flexible Ligand. *Inorganica Chim. Acta* **2015**, *434*, 158–171. https://doi.org/10.1016/j.ica.2015.05.021.
(31) Zhu, L.; Sheng, D.; Xu, C.; Dai, X.; Silver, M. A.; Li, J.; Li, P.; Wang, Y.; Wang, Y.; Chen, L.; Xiao, C.; Chen, J.; Zhou, R.; Zhang, C.; Farha, O. K.; Chai, Z.; Albrecht-Schmitt, T. E.; Wang, S. Identifying the Recognition Site for Selective Trapping of 99TcO4– in a Hydrolytically Stable and Radiation Resistant Cationic Metal–Organic Framework. *J. Am. Chem. Soc.* **2017**, *139* (42), 14873–14876. https://doi.org/10.1021/jacs.7b08632.
(32) Sheng, D.; Zhu, L.; Xu, C.; Xiao, C.; Wang, Y.; Wang, Y.; Chen, L.; Diwu, J.; Chen, J.; Chai, Z.; Albrecht-Schmitt, T. E.; Wang, S. Efficient and Selective Uptake of TcO4– by a Cationic Metal–Organic Framework Material with Open Ag+ Sites. *Environ. Sci. Technol.* **2017**, *51* (6), 3471–3479. https://doi.org/10.1021/acs.est.7b00339.
(33) Zhang, Z.; Xu, L.; Cao, R. Structures and Single Crystal to Single Crystal Transformations of Cadmium Frameworks Using a Flexible Tripodal Ligand. *New J. Chem.* **2018**, *42* (7), 5593–5601. https://doi.org/10.1039/C7NJ05125E.
(34) Zeng, L.-W.; Hu, K.-Q.; Mei, L.; Li, F.-Z.; Huang, Z.-W.; An, S.-W.; Chai, Z.-F.; Shi, W.-Q. Structural Diversity of Bipyridinium-Based Uranyl Coordination Polymers: Synthesis, Characterization, and Ion-Exchange Application. *Inorg. Chem.* **2019**, *58* (20), 14075–14084. https://doi.org/10.1021/acs.inorgchem.9b02106.
(35) Sun, J.-K.; Yang, X.-D.; Yang, G.-Y.; Zhang, J. Bipyridinium Derivative-Based Coordination Polymers: From Synthesis to Materials Applications. *Coord. Chem. Rev.* **2019**, *378*, 533–560. https://doi.org/10.1016/j.ccr.2017.10.029.
(36) Xue, Z.-Z.; Guan, Q.-W.; Xu, L.; Meng, X.-D.; Pan, J. A Zn(II)-Based Coordination Polymer Featuring Selective Detection of Fe3+ and Efficient Capture of Anionic Dyes. *Cryst. Growth Des.* **2020**, *20* (11), 7477–7483. https://doi.org/10.1021/acs.cgd.0c01151.
(37) Zheng, X.; Fan, R.; Xing, K.; Zhu, K.; Wang, P.; Yang, Y. Smart Cationic Coordination Polymer: A Single-Crystal-to-Single-Crystal Approach for Simultaneous Detection and Removal of Perchlorate in Aqueous Media. *Chem. Eng. J.* **2020**, *380*, 122580. https://doi.org/10.1016/j.cej.2019.122580.
(38) Lippi, M.; Cametti, M. Highly Dynamic 1D Coordination Polymers for Adsorption and Separation Applications. *Coord. Chem. Rev.* **2021**, *430*, 213661. https://doi.org/10.1016/j.ccr.2020.213661.
(39) Pahari, G.; Ghosh, S.; Halder, A.; Ghoshal, D. Synthesis of Two Cationic Coordination Polymers for the Exploration of Anion Exchange Properties. *Polyhedron* **2022**, *211*, 115528. https://doi.org/10.1016/j.poly.2021.115528.
(40) Soe, E.; Ehlke, B.; Oliver, S. R. J. A Cationic Silver Pyrazine Coordination Polymer with High Capacity Anion Uptake from Water. *Environ. Sci. Technol.* **2019**, *53* (13), 7663–7672. https://doi.org/10.1021/acs.est.9b01633.
(41) Li, C.-P.; Ai, J.-Y.; He, H.; Li, M.-Z.; Du, M. Divergent Structural Transformations in 3D Ag(I) Porous Coordination Polymers Induced by Solvent and Anion Exchanges. *Cryst. Growth Des.* **2019**, *19* (4), 2235–2244. https://doi.org/10.1021/acs.cgd.8b01843.
(42) Kumar, P.; Pournara, A.; Kim, K.-H.; Bansal, V.; Rapti, S.; Manos, M. J. Metal-Organic Frameworks: Challenges and Opportunities for Ion-Exchange/Sorption Applications. *Prog. Mater. Sci.* **2017**, *86*, 25–74. https://doi.org/10.1016/j.pmatsci.2017.01.002.
(43) K. Cheetham, A.; R. Rao, C. N.; K. Feller, R. Structural Diversity and Chemical Trends in Hybrid Inorganic–Organic Framework Materials. *Chem. Commun.* **2006**, *0* (46), 4780–4795. https://doi.org/10.1039/B610264F.
(44) Shriver, D.; Weller, M.; Overton, T.; Rourke, J.; Armstrong, F. *Inorganic Chemistry*, 6th ed.; Oxford University Press, 2014.

(45) Huang, Z.; Du, M.; Song, H.-B.; Bu, X.-H. Effect of Anions on the Framework Formation of Novel AgI Coordination Polymers with Angular Bridging Ligands. *Cryst. Growth Des.* **2004**, *4* (1), 71–78. https://doi.org/10.1021/cg0341095.
(46) Park, K.-M.; Seo, J.; Moon, S.-H.; Lee, S. S. Stepwise Synthesis of Charged and Neutral Two-Dimensional Networks via One-Dimensional Silver(I) Coordination Polymer Based on Bis(4-Pyridylmethyl)Sulfide. *Cryst. Growth Des.* **2010**, *10* (9), 4148–4154. https://doi.org/10.1021/cg1008472.
(47) Michaelides, A.; Skoulika, S. Anion-Induced Formation of Lanthanide-Organic Chains From 3D Framework Solids. Anion Exchange in a Crystal-to-Crystal Manner. *Cryst. Growth Des.* **2009**, *9* (5), 2039–2042. https://doi.org/10.1021/cg801138e.
(48) Toh, N. L.; Nagarathinam, M.; Vittal, J. J. Topochemical Photodimerization in the Coordination Polymer [{(CF3CO2)(?-O2CCH3)Zn}2(?-Bpe)2]n through Single-Crystal to Single-Crystal Transformation. *Angew. Chem. Int. Ed.* **2005**, *44* (15), 2237–2241. https://doi.org/10.1002/anie.200462673.
(49) Theiss, F. L.; Couperthwaite, S. J.; Ayoko, G. A.; Frost, R. L. A Review of the Removal of Anions and Oxyanions of the Halogen Elements from Aqueous Solution by Layered Double Hydroxides. *J. Colloid Interface Sci.* **2014**, *417*, 356–368. https://doi.org/10.1016/j.jcis.2013.11.040.
(50) Wu, X.; Wang, Y.; Xu, L.; Lv, L. Removal of Perchlorate Contaminants by Calcined Zn/Al Layered Double Hydroxides: Equilibrium, Kinetics, and Column Studies. *Desalination* **2010**, *256* (1), 136–140. https://doi.org/10.1016/j.desal.2010.02.001.
(51) Celik, A.; Roy, S. C.; Quintero, M. A.; Taylor-Pashow, K.; Li, D.; Kanatzidis, M. G.; Zhu, X.; Islam, S. M. Unveiling the Potential of [Sn2S6]4– Functionalized Layered Double Hydroxides for the Sorption of ReO4– as a Surrogate for 99TcO4–. *ACS Appl. Eng. Mater.* **2023**, *1* (7), 1711–1718. https://doi.org/10.1021/acsaenm.3c00074.
(52) Tanaka, K.; Kozai, N.; Yamasaki, S.; Ohnuki, T.; Kaplan, D. I.; Grambow, B. Adsorption Mechanism of ReO4− on Ni–Zn Layered Hydroxide Salt and Its Application to Removal of ReO4− as a Surrogate of TcO4−. *Appl. Clay Sci.* **2019**, *182*, 105282. https://doi.org/10.1016/j.clay.2019.105282.
(53) Tran, H. N.; Nguyen, D. T.; Le, G. T.; Tomul, F.; Lima, E. C.; Woo, S. H.; Sarmah, A. K.; Nguyen, H. Q.; Nguyen, P. T.; Nguyen, D. D.; Nguyen, T. V.; Vigneswaran, S.; Vo, D.-V. N.; Chao, H.-P. Adsorption Mechanism of Hexavalent Chromium onto Layered Double Hydroxides-Based Adsorbents: A Systematic in-Depth Review. *J. Hazard. Mater.* **2019**, *373*, 258–270. https://doi.org/10.1016/j.jhazmat.2019.03.018.
(54) C. Rohit, R.; Chandra Roy, S.; Alam, R.; M. Islam, S. Metal-Sulfide/Polysulfide Functionalized Layered Double Hydroxides – Recent Progress in the Removal of Heavy Metal Ions and Oxoanionic Species from Aqueous Solutions. *Dalton Trans.* **2024**, *53* (24), 10037–10049. https://doi.org/10.1039/D4DT00883A.
(55) Kim, Y.; Son, Y.; Bae, S.; Kim, T.-H.; Hwang, Y. Particle Size and Interlayer Anion Effect on Chromate Adsorption by MgAl-Layered Double Hydroxide. *Appl. Clay Sci.* **2022**, *225*, 106552. https://doi.org/10.1016/j.clay.2022.106552.
(56) Cui, X.; Khlobystov, A. N.; Chen, X.; Marsh, D. H.; Blake, A. J.; Lewis, W.; Champness, N. R.; Roberts, C. J.; Schröder, M. Dynamic Equilibria in Solvent-Mediated Anion, Cation and Ligand Exchange in Transition-Metal Coordination Polymers: Solid-State Transfer or Recrystallisation? *Chem. - Eur. J.* **2009**, *15* (35), 8861–8873. https://doi.org/10.1002/chem.200900796.
(57) N. Adarsh, N.; Dastidar, P. Coordination Polymers : What Has Been Achieved in Going from Innocent 4,4'-Bipyridine to Bis-Pyridyl Ligands Having a Non-Innocent Backbone? *Chem. Soc. Rev.* **2012**, *41* (8), 3039–3060. https://doi.org/10.1039/C2CS15251G.

(58) Novendra, N.; Marrett, J. M.; Katsenis, A. D.; Titi, H. M.; Arhangelskis, M.; Friščić, T.; Navrotsky, A. Linker Substituents Control the Thermodynamic Stability in Metal–Organic Frameworks. *J. Am. Chem. Soc.* **2020**, *142* (52), 21720–21729. https://doi.org/10.1021/jacs.0c09284.
(59) Boag, N. M.; Coward, K. M.; Jones, A. C.; Pemble, M. E.; Thompson, J. R. 4,4'-Bipyridyl at 203K. *Acta Crystallogr. C* **1999**, *55* (4), 672–674. https://doi.org/10.1107/S0108270198016333.
(60) Ji, W.; Xue, B.; Bera, S.; Guerin, S.; Liu, Y.; Yuan, H.; Li, Q.; Yuan, C.; Shimon, L. J. W.; Ma, Q.; Kiely, E.; Tofail, S. A. M.; Si, M.; Yan, X.; Cao, Y.; Wang, W.; Yang, R.; Thompson, D.; Li, J.; Gazit, E. Tunable Mechanical and Optoelectronic Properties of Organic Cocrystals by Unexpected Stacking Transformation from H- to J- and X-Aggregation. *ACS Nano* **2020**, *14* (8), 10704–10715. https://doi.org/10.1021/acsnano.0c05367.
(61) Lv, X.-L.; Yuan, S.; Xie, L.-H.; Darke, H. F.; Chen, Y.; He, T.; Dong, C.; Wang, B.; Zhang, Y.-Z.; Li, J.-R.; Zhou, H.-C. Ligand Rigidification for Enhancing the Stability of Metal–Organic Frameworks. *J. Am. Chem. Soc.* **2019**, *141* (26), 10283–10293. https://doi.org/10.1021/jacs.9b02947.
(62) Wang, K.; Lv, X.-L.; Feng, D.; Li, J.; Chen, S.; Sun, J.; Song, L.; Xie, Y.; Li, J.-R.; Zhou, H.-C. Pyrazolate-Based Porphyrinic Metal–Organic Framework with Extraordinary Base-Resistance. *J. Am. Chem. Soc.* **2016**, *138* (3), 914–919. https://doi.org/10.1021/jacs.5b10881.
(63) Ding, M.; Cai, X.; Jiang, H.-L. Improving MOF Stability: Approaches and Applications. *Chem. Sci.* **2019**, *10* (44), 10209–10230. https://doi.org/10.1039/C9SC03916C.
(64) Yuan, S.; Feng, L.; Wang, K.; Pang, J.; Bosch, M.; Lollar, C.; Sun, Y.; Qin, J.; Yang, X.; Zhang, P.; Wang, Q.; Zou, L.; Zhang, Y.; Zhang, L.; Fang, Y.; Li, J.; Zhou, H.-C. Stable Metal–Organic Frameworks: Design, Synthesis, and Applications. *Adv. Mater.* **2018**, *30* (37), 1704303. https://doi.org/10.1002/adma.201704303.
(65) Zhong, D.; Lu, T. Porous Coordination Polymers Based on Three Planar Rigid Ligands. *Sci. China Chem.* **2011**, *54* (9), 1395–1406. https://doi.org/10.1007/s11426-011-4358-z.
(66) Wang, J.; Guo, X. Adsorption Kinetic Models: Physical Meanings, Applications, and Solving Methods. *J. Hazard. Mater.* **2020**, *390*, 122156. https://doi.org/10.1016/j.jhazmat.2020.122156.
(67) Revellame, E. D.; Fortela, D. L.; Sharp, W.; Hernandez, R.; Zappi, M. E. Adsorption Kinetic Modeling Using Pseudo-First Order and Pseudo-Second Order Rate Laws: A Review. *Clean. Eng. Technol.* **2020**, *1*, 100032. https://doi.org/10.1016/j.clet.2020.100032.
(68) Sheldrick, G. M. A Short History of SHELX. *Acta Crystallogr. A* **2008**, *64* (1), 112–122. https://doi.org/10.1107/S0108767307043930.
(69) Dolomanov, O. V.; Bourhis, L. J.; Gildea, R. J.; Howard, J. a. K.; Puschmann, H. OLEX2: A Complete Structure Solution, Refinement and Analysis Program. *J. Appl. Crystallogr.* **2009**, *42* (2), 339–341. https://doi.org/10.1107/S0021889808042726.
(70) Müller, P. Practical Suggestions for Better Crystal Structures. *Crystallogr. Rev.* **2009**, *15* (1), 57–83. https://doi.org/10.1080/08893110802547240.
(71) Macrae, C. F.; Sovago, I.; Cottrell, S. J.; Galek, P. T. A.; McCabe, P.; Pidcock, E.; Platings, M.; Shields, G. P.; Stevens, J. S.; Towler, M.; Wood, P. A. Mercury 4.0: From Visualization to Analysis, Design and Prediction. *J. Appl. Crystallogr.* **2020**, *53* (1), 226–235. https://doi.org/10.1107/S1600576719014092.
(72) Momma, K.; Izumi, F. VESTA 3 for Three-Dimensional Visualization of Crystal, Volumetric and Morphology Data. *J. Appl. Crystallogr.* **2011**, *44* (6), 1272–1276. https://doi.org/10.1107/S0021889811038970.
(73) Giannozzi, P.; Baroni, S.; Bonini, N.; Calandra, M.; Car, R.; Cavazzoni, C.; Ceresoli, D.; Chiarotti, G. L.; Cococcioni, M.; Dabo, I.; Corso, A. D.; Gironcoli, S. de; Fabris, S.; Fratesi, G.; Gebauer, R.; Gerstmann, U.; Gougoussis, C.; Kokalj, A.; Lazzeri, M.; Martin-Samos, L.; Marzari, N.; Mauri, F.; Mazzarello, R.; Paolini, S.; Pasquarello, A.; Paulatto, L.; Sbraccia, C.; Scandolo, S.; Sclauzero, G.; Seitsonen, A. P.; Smogunov, A.; Umari, P.; Wentzcovitch, R. M. QUANTUM ESPRESSO: A Modular

and Open-Source Software Project for Quantum Simulations of Materials. *J. Phys. Condens. Matter* **2009**, *21* (39), 395502. https://doi.org/10.1088/0953-8984/21/39/395502.
(74) Kresse, G.; Joubert, D. From Ultrasoft Pseudopotentials to the Projector Augmented-Wave Method. *Phys. Rev. B* **1999**, *59* (3), 1758–1775. https://doi.org/10.1103/PhysRevB.59.1758.
(75) Blöchl, P. E. Projector Augmented-Wave Method. *Phys. Rev. B* **1994**, *50* (24), 17953–17979. https://doi.org/10.1103/PhysRevB.50.17953.
(76) Perdew, J. P.; Burke, K.; Ernzerhof, M. Generalized Gradient Approximation Made Simple. *Phys. Rev. Lett.* **1996**, *77* (18), 3865–3868. https://doi.org/10.1103/PhysRevLett.77.3865.
(77) Dal Corso, A. Pseudopotentials Periodic Table: From H to Pu. *Comput. Mater. Sci.* **2014**, *95*, 337–350. https://doi.org/10.1016/j.commatsci.2014.07.043.
(78) Kokunov, Yu. V.; Gorbunova, Yu. E.; Khmelevskaya, L. V. Synthesis and Crystal Structure of the Coordination Polymer of Silver with 4,4′-Bipyridylethylene [Ag(Bpe)](NO3)·3H2O. *Russ. J. Inorg. Chem.* **2006**, *51* (8), 1192–1197. https://doi.org/10.1134/S0036023606080079.
(79) Yaghi, O. M.; Li, H. T-Shaped Molecular Building Units in the Porous Structure of Ag(4,4′-Bpy)·NO3. *J. Am. Chem. Soc.* **1996**, *118* (1), 295–296. https://doi.org/10.1021/ja953438l.
(80) Lin, H.; Wu, X.; Maggard, P. A. Ligand-Based Modification of the Structures and Optical Properties of New Silver(I)-Rhenate(VII) Oxide/Organic Hybrid Solids. *Inorg. Chem.* **2009**, *48* (23), 11265–11276. https://doi.org/10.1021/ic901749r.
(81) Hu, X.-M.; Li, F.-A. Catena-Poly[[Tris[Silver(I)-μ-4,4′-Bi-pyridine-κ2N:N′]] Tris-(Perchlorate) Di-hydrate]. *Acta Crystallogr. Sect. E Struct. Rep. Online* **2011**, *67* (11), m1505–m1505. https://doi.org/10.1107/S1600536811040153.
(82) R. Martinez, C.; L. Iverson, B. Rethinking the Term “Pi-Stacking.” *Chem. Sci.* **2012**, *3* (7), 2191–2201. https://doi.org/10.1039/C2SC20045G.
(83) Michalczyk, M.; Zierkiewicz, W.; Drożdżewski, P.; Nawaz, S.; Monim-ul-Mehboob, M.; Ahmad, S. Theoretical Modeling of Argentophilic Interactions in [Ag(CN)2−]3 Trimer Found in a Copper(II) Complex of *Cis*-1,2-Diaminocyclohexane (Dach), [Cu(Dach)2-Ag(CN)2-Cu(Dach)2][Ag(CN)2]3. *Chem. Phys. Lett.* **2018**, *709*, 11–15. https://doi.org/10.1016/j.cplett.2018.08.034.
(84) Schmidbaur, H.; Schier, A. Argentophilic Interactions. *Angew. Chem. Int. Ed.* **2015**, *54* (3), 746–784. https://doi.org/10.1002/anie.201405936.
(85) Groom, C. R.; Bruno, I. J.; Lightfoot, M. P.; Ward, S. C. The Cambridge Structural Database. *Acta Crystallogr. Sect. B Struct. Sci. Cryst. Eng. Mater.* **2016**, *72* (2), 171–179. https://doi.org/10.1107/S2052520616003954.
(86) Bruno, I. J.; Cole, J. C.; Edgington, P. R.; Kessler, M.; Macrae, C. F.; McCabe, P.; Pearson, J.; Taylor, R. New Software for Searching the Cambridge Structural Database and Visualizing Crystal Structures. *Acta Crystallogr. B* **2002**, *58* (3), 389–397. https://doi.org/10.1107/S0108768102003324.
(87) Hackert, M. L.; Jacobson, R. A. The Crystal Structure of Silver Chromate. *J. Solid State Chem.* **1971**, *3* (3), 364–368. https://doi.org/10.1016/0022-4596(71)90072-7.
(88) Naumov, D. Y.; Virovets, A. V.; Korenev, S. V.; Gubanov, A. I. Silver Perrhenate, AgReO4. *Acta Crystallogr. C* **1999**, *55* (8). https://doi.org/10.1107/S0108270199099138.
(89) Goreshnik, E.; Mazej, Z. X-Ray Single Crystal Structure and Vibrational Spectra of AgBF4. *Solid State Sci.* **2005**, *7* (10), 1225–1229. https://doi.org/10.1016/j.solidstatesciences.2005.06.007.
(90) Meyer, P.; Rimsky, A.; Chevalier, R. Structure du nitrate d’argent à pression et température ordinaires. Exemple de cristal parfait. *Acta Crystallogr. B* **1978**, *34* (5), 1457–1462. https://doi.org/10.1107/S0567740878005907.
(91) Olson, L. P.; Whitcomb, D. R.; Rajeswaran, M.; Blanton, T. N.; Stwertka, B. J. The Simple Yet Elusive Crystal Structure of Silver Acetate and the Role of the Ag−Ag Bond in the Formation of Silver Nanoparticles during the Thermally Induced Reduction of Silver Carboxylates. *Chem. Mater.* **2006**, *18* (6), 1667–1674. https://doi.org/10.1021/cm052657v.

(92) Berthold, H. J.; Ludwig, W.; Wartchow, R. Verfeinerung der Kristallstruktur des Silberperchlorats AgClO4. *Z. Für Krist. - Cryst. Mater.* **1979**, *149* (1–4), 327–336. https://doi.org/10.1524/zkri.1979.149.14.327.
(93) Pérez-Jiménez, Á. J.; Sancho-García, J. C.; Pérez-Jordá, J. M. Torsional Potential of 4,4'-Bipyridine: Ab Initio Analysis of Dispersion and Vibrational Effects. *J. Chem. Phys.* **2005**, *123* (13), 134309. https://doi.org/10.1063/1.2043107.
(94) Bâldea, I.; Köppel, H.; Wenzel, W. (4,4')-Bipyridine in Vacuo and in Solvents : A Quantum Chemical Study of a Prototypical Floppy Molecule from a Molecular Transport Perspective. *Phys. Chem. Chem. Phys.* **2013**, *15* (6), 1918–1928. https://doi.org/10.1039/C2CP43627B.
(95) Cacelli, I.; Cimoli, A.; Livotto, P. R.; Prampolini, G. An Automated Approach for the Parameterization of Accurate Intermolecular Force-Fields: Pyridine as a Case Study. *J. Comput. Chem.* **2012**, *33* (10), 1055–1067. https://doi.org/10.1002/jcc.22937.
(96) Ali, I.; Ahmed, B.; Barukial, P.; Bezbaruah, M. J.; Upadhyaya, M.; Talukdar, A.; Das, K.; Bezbaruah, B. A Comparative DFT Study on the π-π Stacking Interaction of Some N-Based Organic Fused Heterocycles with Eclipsed and Staggered Conformations. *J. Indian Chem. Soc.* **2022**, *99* (10), 100698. https://doi.org/10.1016/j.jics.2022.100698.
(97) Mishra, B. K.; Sathyamurthy, N. Π−π Interaction in Pyridine. *J. Phys. Chem. A* **2005**, *109* (1), 6–8. https://doi.org/10.1021/jp045218c.
(98) Kuśmierek, K., Świątkowski, A. The Influence of Different Agitation Techniques on the Adsorption Kinetics of 4-Chlorophenol on Granular Activated Carbon. *React. Kinet. Mech. Cat.* **2015**, *116*, 267–271. https://doi.org/10.1007/s11144-015-0889-1.
(99) Jaiswal, K. S.; Rathod, V. K. Enzymatic Synthesis of Cosmetic Grade Wax Ester in Solvent Free System: Optimization, Kinetic and Thermodynamic Studies. *SN Appl. Sci.* **2019**, *1* (8), 949. https://doi.org/10.1007/s42452-019-0955-9.
(100) *CRC Handbook of Chemistry and Physics*, 97th ed.; Haynes, W. M., Lide, D. R., Bruno, T. J., Eds.; CRC Press/Taylor and Francis, 2016.
(101) Robin, A. Y.; Fromm, K. M. Coordination Polymer Networks with O- and N-Donors: What They Are, Why and How They Are Made. *Coord. Chem. Rev.* **2006**, *250* (15), 2127–2157. https://doi.org/10.1016/j.ccr.2006.02.013.
(102) Clark, R. W.; Bonicamp, J. M. The Ksp-Solubility Conundrum. *J. Chem. Educ.* **1998**, *75* (9), 1182. https://doi.org/10.1021/ed075p1182.
(103) Parashar, R.; Parashar, R. *The Role of Common Lon and Adverse Ion in Analytical Chemistry*; 2003.
(104) Suh, I.-K.; Ohta, H.; Waseda, Y. High-Temperature Thermal Expansion of Six Metallic Elements Measured by Dilatation Method and X-Ray Diffraction. *J. Mater. Sci.* **1988**, *23* (2), 757–760. https://doi.org/10.1007/BF01174717.
(105) Ralph W. G. Wyckoff. *Crystal Structures*, 2nd ed.; Interscience Publishers, 1963; Vol. 1.
(106) Häglund, J.; Fernández Guillermet, A.; Grimvall, G.; Körling, M. Theory of Bonding in Transition-Metal Carbides and Nitrides. *Phys. Rev. B* **1993**, *48* (16), 11685–11691. https://doi.org/10.1103/PhysRevB.48.11685.

For Table of Contents Use Only

TOC Image:

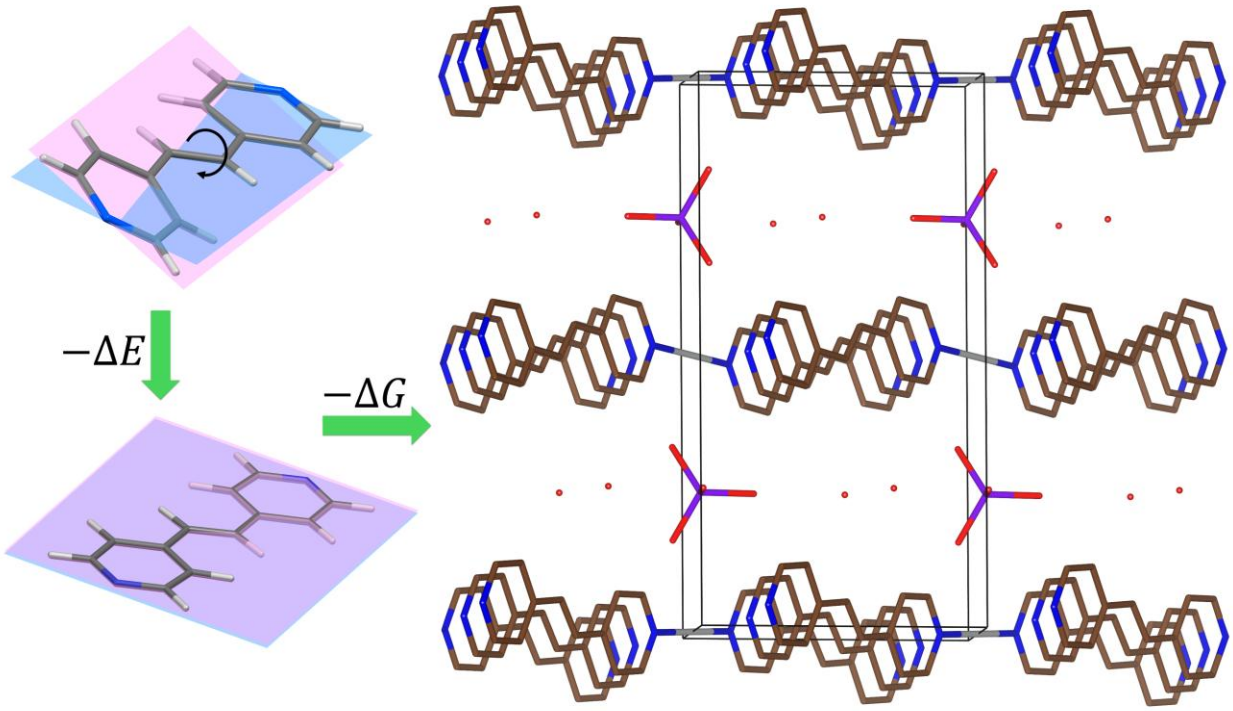

Synopsis: We present new cationic coordination polymers with superior aqueous formation energies by ligand replacement.